NUMERICAL ANALYSIS OF SUPERCRITICAL FLOW INSTABILITIES IN A NATURAL CIRCULATION LOOP

BY

PRASHANT KUMAR JAIN

B.Tech., Indian Institute of Technology Bombay, 2004

THESIS

Submitted in partial fulfillment of the requirements
for the degree of Master of Science in Nuclear Engineering
in the Graduate College of the
University of Illinois at Urbana-Champaign, 2006

Urbana, Illinois

Abstract

NUMERICAL ANALYSIS OF SUPERCRITICAL FLOW INSTABILITIES IN A NATURAL CIRCULATION LOOP

Prashant K Jain, M.S.
Department of Nuclear, Plasma and Radiological Engineering
University of Illinois at Urbana-Champaign, 2006
Rizwan-uddin, Adviser

Numerical studies have been carried out to investigate flow instabilities in a natural circulation loop with supercritical fluid (H_2O, CO_2). For steady state and dynamic analyses of the loop under supercritical conditions, a single-channel, one-dimensional model is developed. In this model, equations for the conservation of mass, momentum and energy are discretized using an implicit finite difference scheme. A computer code called FIASCO (Flow Instability Analysis under SuperCritical Operating conditions) is developed in FORTRAN90 to simulate the dynamics of natural circulation loops with supercritical fluid. Stability boundary results for the CO_2 natural circulation loop substantially deviate from the results reported by previous investigators, and contradict some of the reported findings. The disagreement in results is most likely due to the undesirable dissipative and dispersive effects produced from the large time steps used in previous studies, thereby leading to a larger stable region than those found using smaller time steps. Results presented in this thesis suggest that the stability boundary of a natural circulation loop with supercritical fluid is not confined to the *near-peak region* of the (steady state) flow-power curve. Additional and more extensive experimental data are needed to resolve the differences between results obtained here and those reported earlier. However, results obtained for the range of parameter values used in this investigation always predict the stability threshold to be in the positive slope region of the (steady

state) flow-power curve. Parametric studies for different operating conditions reveal the similarity of stability characteristics under supercritical conditions with those in two-phase flows.

Acknowledgement

I wish to take this opportunity to express my sincere gratitude towards my advisor Professor Rizwan-uddin for his valuable support throughout the project work. Without his insight, guidance and encouragement; this work would not have taken its present shape. I am very much looking forward to continuing my graduate studies towards doctoral degree under his supervision. I would also like to thank Professor Barclay Jones for serving as the reader for this thesis.

I would also like to thank my family for their support and encouragement; without their love and patience, none of this would have been possible. Also, I would like to extend thanks to Suneet Singh for his academic help and assistance, which has proved invaluable during my stay here at the department. I would also like to appreciate: Bei Ye, Lifeng Gu, and Hitesh Bindra, for their friendship and technical assistance in several course projects. Finally, I would like to acknowledge all the faculty and staff of NPRE for their immense support, guidance, and wisdom.

Prashant K Jain

Table of contents

List of Figures

Nomenclature

C_k	coefficient in momentum conservation equation
D_h	hydraulic diameter, m
f	friction coefficient
g	acceleration due to gravity, m/s^2
h	specific enthalpy, J/kg
i	grid index
m	index for the last grid point
n	time step index
p	pressure, N/m^2
q'''	volumetric heat addition rate, W/m^3
Re	Reynolds number
R_{k_1}	inlet restriction coefficient
R_{k_2}	exit restriction coefficient
t	time, s
u	velocity, m/s
z	axial distance, m
ρ	density, kg/m^3
θ	angle of flow direction with respect to horizontal plane, rad
μ	dynamic viscosity, $N\text{-}s/m^2$
η	$=\dfrac{\Delta z}{2\Delta t}$
Δz	spatial grid size, m
Δt	time step size, s

Chapter 1

Introduction

Supercritical-Water-Cooled Reactor (SCWR) is one of the advanced nuclear reactor systems selected under the Generation IV program for cost effective energy generation, and safety. The SCWR concept, which evolved from the Japanese supercritical light water reactor (SCLWR), has a thermal neutron spectrum, and is cooled and moderated by supercritical light water. This design is built upon two well developed technologies: Light Water Reactors (LWRs) and supercritical fossil-fired boilers. This reactor system may have potential to improve fuel economy and may simplify plant design considerably. Moreover, compared with the LWRs, higher thermal efficiency and lower coolant mass flow rate *per unit core thermal power* can be achieved with SCWRs (Yamaji et al., 2005). It is also rated good in safety, proliferation resistance and physical protection because of its passive safety features, designed to avoid accidents and reduced operator dependability (GIF, 2002).

In SCWR, operation at supercritical pressure (25.0 MPa) eliminates coolant boiling, so the coolant always remains in single-phase throughout the system; and superheated steam can be obtained without the danger of dryout in the core. However, a gradual deterioration in heat transfer may occur in the *near-critical region* (narrow region around the pseudo-critical point), but does not result in significant drop in the heat transfer coefficients associated with dryout (Pioro et al., 2004). Additionally, employment of single-loop cycle remarkably simplifies the nuclear system eliminating the need of recirculation lines, pressurizer, steam separators and dryers, as coolant directly circulates to and fro from the core to the turbine (see Figure 1.1). [A comparison among different type of reactor systems is shown in Figure 1.2.] In short, SCWR design takes advantage of the desirable feature of BWR over PWR (single loop) without the associated disadvantage (boiling). Moreover, the mass flow rate of coolant in SCWR is low, and

core exit temperature is high with a large temperature increase across the core, thereby resulting in a high plant thermal efficiency of about 44% (Yamaji et al., 2005).

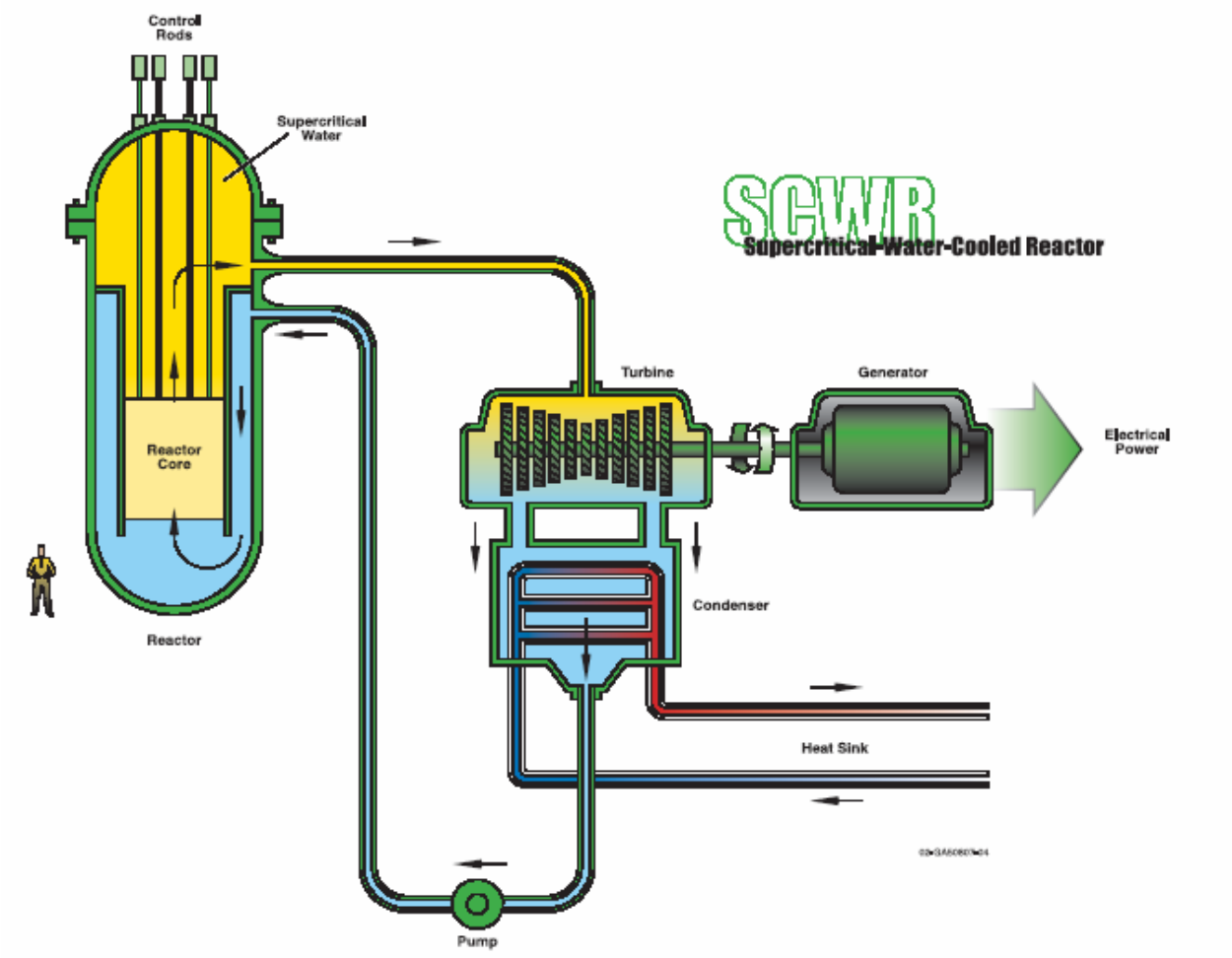

Figure 1.1: SCWR simplified flow diagram (GIF, 2002)

Due to supercritical operating conditions in SCWR, thermodynamic and transport properties of water change significantly as its temperature approaches the pseudocritical point, where the distinction between liquid and vapor phases disappears. The heat conduction coefficient and the heat capacity at constant pressure tend to increase dramatically, while the thermal diffusivity tends to zero (Zappoli, 2003). Also, density and viscosity tend to decrease significantly as fluid temperature approaches the pseudocritical point. Some of these dramatic variations in thermophysical properties of supercritical water (at 25 MPa) are shown in Figure 1.3 as a function of temperature.

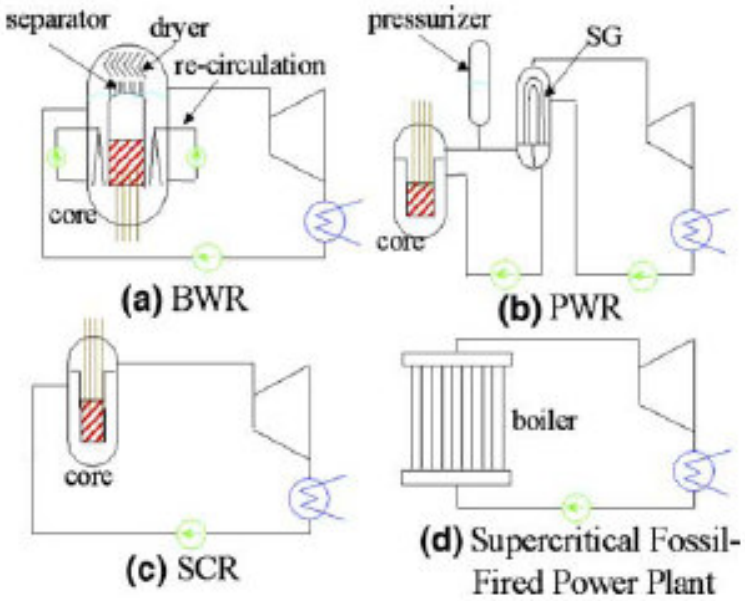

Figure 1.2: Comparison of different plant systems (Yamaji et al., 2005)

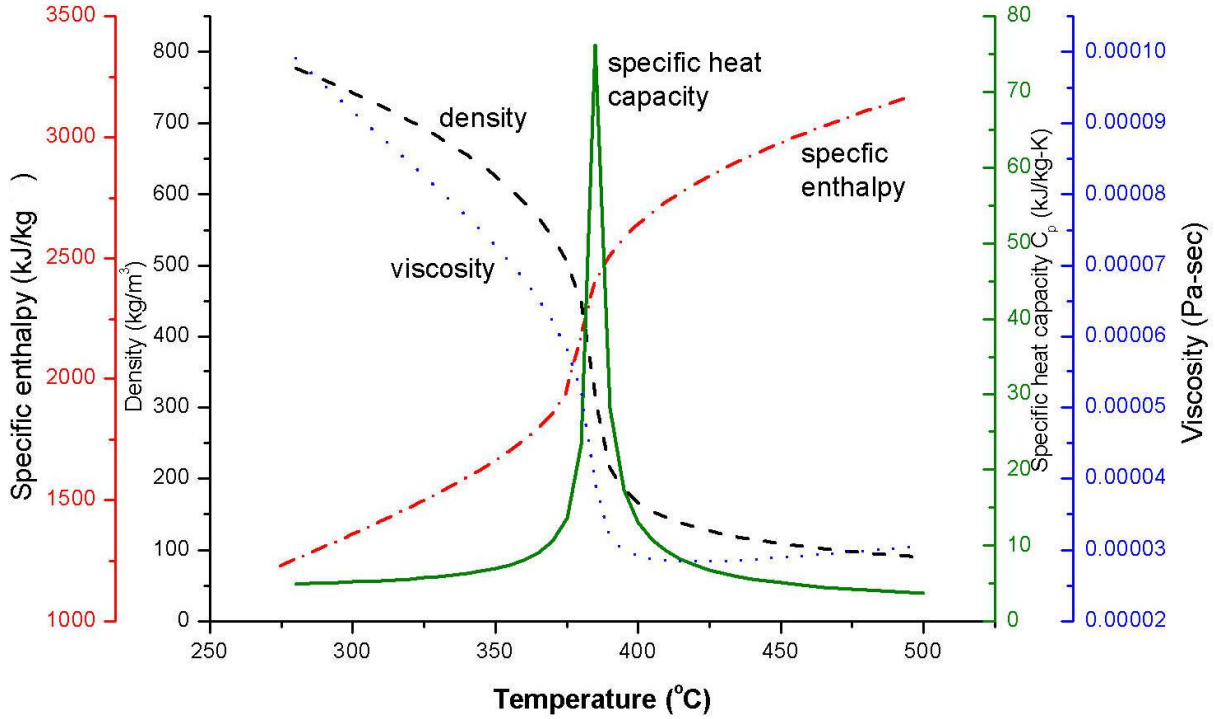

Figure 1.3: Physical properties of superciritical water at 25 MPa

It may be observed that the density decreases from 800 kg/m^3 at the core inlet (~280 C) to less than 100 kg/m^3 at the core outlet (~ 450─500 C). Corresponding specific enthalpy change is nearly 2000 kJ/kg. A comparison among operating conditions of the Supercritical Water Reactor (SCWR), Pressurized Water Reactor (PWR) and Boiling Water Reactor (BWR) are shown in pressure-temperature and temperature-entropy diagrams of Figure 1.4. It is apparent from this figure that in the SCWR design there is no phase transition (i.e. no two phase) of water as its temperature crosses the pseudo-critical point.

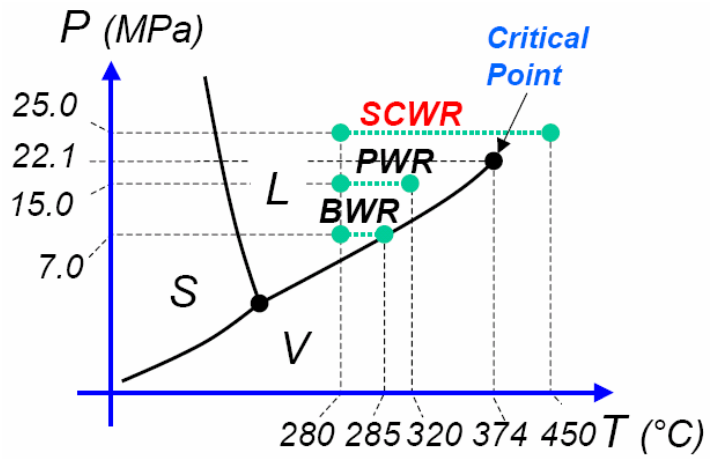

(a)

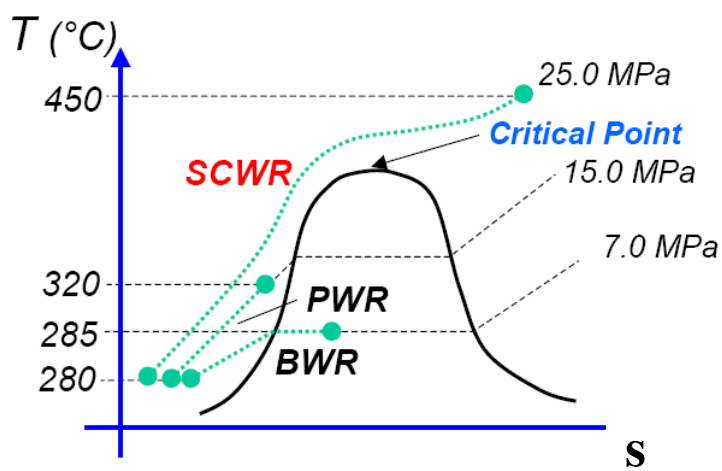

(b)

Figure 1.4: Comparison of operating conditions of the SCWR, PWR and BWR (Buongiorno, 2004)

Similar to BWRs, SCWR core will experience large changes in density across the core and for this reason may be susceptible to flow instabilities similar to those observed in BWRs (such as density-wave instabilities, and coupled thermohydraulic and neutronic instabilities). In addition, dramatic changes in other thermophysical properties may also lead to yet unexplored phenomena. Therefore, the licensing of SCWR will require demonstrable capability to predict the onset of instabilities. Consequently, it is necessary to understand the instability phenomena in SCWR and identify the variables which affect these phenomena. The ultimate goal is to generate stability maps to identify stable operating conditions for SCWR design.

These anticipated instabilities in SCWR may be *static* or *dynamic* in nature. If perturbation at the steady state condition leads towards a different steady state operating condition, then the flow system is considered to be under *static* flow instability. Threshold for this type of instability can be predicted by using only the steady state governing equations. Flow is subject to *dynamic* instability, if due to inertia and other feedback effects, small perturbations in the steady state condition lead towards sustained or diverging flow oscillations. Threshold for this type of instability can not be predicted by solving the steady state equations only; time-dependent (dynamic) conservation equations must be solved in order to identify the threshold for dynamic instabilities (Tong and Tang, 1997).

Thermal hydraulic instabilities resulting in flow oscillations will be highly undesirable in SCWR system, as they may give rise to: 1) nuclear instabilities (due to density-reactivity feedback); 2) result in failure of control mechanism; or 3) fatigue damage of reactor components. A drop in the heat removal system efficiency may put the safety of reactor system in jeopardy. Moreover, emphasis is also placed on passive safety mechanisms by employing, for example, natural circulation cooling systems (rather than forced ones) to remove core decay heat after accidental reactor shutdown. Consequently, it is necessary to study SCWR stability under natural circulation conditions.

The natural circulation loop with supercritical flow conditions ─ that always remains in single phase ─ experiences a rather large density change across a very small temperature range near the pseudo-critical point. This may lead the system towards instabilities similar to those observed in heated channels with two-phase flows. Instabilities in loops with supercritical flow, associated with the two-phase-like property variation of single phase supercritical fluid, near the pseudocritical point have not been fully explored. A review of some of the recent work is presented in the next chapter. Hence, a study of flow stability phenomena in a natural circulation loop with supercritical fluid is carried out in this thesis, which may later be modified to analyze SCWR instabilities as well.

Since the motivation for the stability analysis of SCWRs is driven by the experience with two-phase flow and BWRs, in the following section, various flow instabilities observed in heated channels with two-phase flows and BWRs (that may also be relevant to SCWRs) are briefly classified and their physical mechanisms explained.

1.1 Classification of flow instabilities

Flow instabilities are usually caused by a feedback mechanism that leads to a reinforcement of perturbations and strongly depend on the thermo-hydrodynamic behavior and geometric configuration of the system. These instabilities usually originate from small amplitude perturbations and lead to a different operating point, growing amplitude oscillations or self sustained oscillations. Researchers have categorized these instabilities in several different ways. Broadly, these flow instabilities have been classified as static or dynamic, and may be *simple* or *compound* in nature (Boure et al, 1973). Instability is *simple*, if it can be explained completely in terms of a single mechanism and does not depend upon interaction of different flow governing processes, such as flow excursion instability or density wave oscillations. Whereas, *compound* instability is the result of several elementary mechanisms and cannot be studied separately. Examples of compound instability include BWR instability and thermal oscillations (Tong and Tang, 1997). Further categorization of flow instabilities is based

on the type of instability mechanisms. These are summarized in Figure A.1 (Jain, 2005) in Appendix A.

Due to of the fact that density wave instabilities are of most concern in BWRs and are likely to be of concern in the SCWR design, it is of interest to discuss them in detail. Physical mechanisms behind density wave oscillations and observed parametric effects are discussed in the following sections.

1.2 Physical mechanism behind density wave instability

Most probable instabilities in commercial BWRs – *channel flow instability* and *coupled neutronic-thermohydraulic instability* – have their "roots" in the density wave mechanism and are illustrated in Figure 1.5 (Leuba and Rey, 1993).

In commercial BWRs, the coolant flows in the upward direction through the core which can be approximated by a heated channel. Usually, flow in a heated channel is due to an externally imposed pressure drop and the fluid at the channel inlet is subcooled. Heat addition along the channel length causes the flowing liquid to boil and, thus, the variation or perturbations in density (in the bottom part of the channel) travel upwards with the flow, giving rise to density wave oscillations.

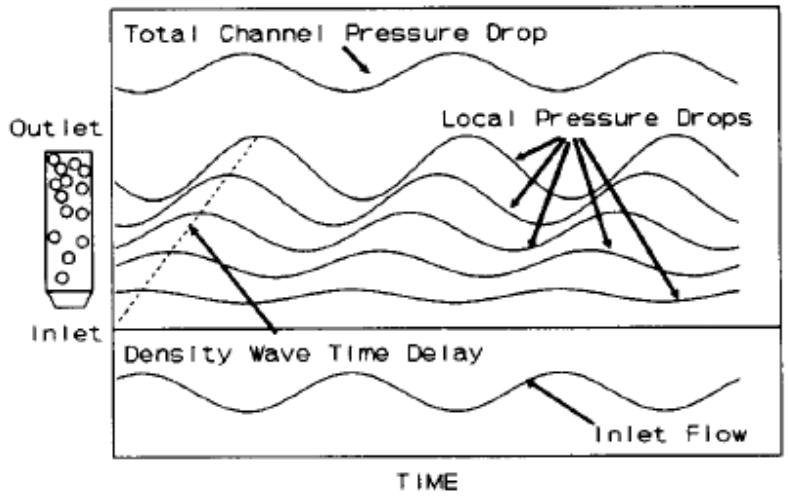

Figure 1.5: Density wave mechanism (Leuba and Rey, 1993)

Suppose, due to some perturbations, inlet flow is reduced for a small time interval while other operating parameters (such as channel power, inlet pressure and temperature) are held constant. This will increase the temperature in the single phase region, move the boiling boundary downwards and increase the voids in the bottom part of the channel. These voids will travel upwards, as a packet, forming a propagating density wave. This, in turn, will affect the local pressure drop at each axial location along the heated channel, which is delayed by the *density wave propagation time*. As local pressure drop in the two-phase region, which is very sensitive to the local void-fraction, is increased due to the extra amount of void, the effect of the perturbation on the total pressure drop is delayed with respect to the original perturbation. In Figure 1.5, the inlet flow is perturbed sinusoidally which results in delayed sinusoidal local pressure drops. Adding these, yield out-of-phase pressure oscillations at the channel exit (Leuba and Rey, 1993). If the pressure drop across the channel is held fixed, it is the inlet flow rate that oscillates to compensate for the variation in local (distributed) pressure drops. Density wave instabilities are, sometimes, also referred to as "flow-void feedback instabilities" and "time-delay instabilities" (Boure et al., 1973).

1.3 Parametric effects on density wave instability

Parametric effects on density wave instability are discussed in the following sub-sections, providing further insight to better understand parameter dependency of natural circulation flow instability under supercritical conditions.

1.3.1 Effect of pressure

For a given input power, increasing system pressure reduces the void fraction and that, in turn, decreases the two-phase flow friction and momentum pressure drops and, thus, stabilizes the system (Boure et al, 1973).

1.3.2 Effect of inlet and exit restrictions

An inlet restriction increases single-phase friction, which provides a damping effect on the increasing flow and thereby increases flow stability. On the other hand, an exit restriction increases two-phase friction (which is out-of-phase with the inlet perturbations) and thereby reduces flow stability (Boure et al, 1973).

1.3.3 Effect of inlet subcooling

An increase in inlet subcooling from medium or high levels results in increasing non-boiling length and reducing the void fraction and, thus, stabilizes the flow system. Whereas, an increase in inlet subcooling from a small value destabilizes the flow due to significant incremental change of transit time (Boure et al, 1973).

1.3.4 Effect of channel length

It was observed during some experimental investigations that the reduction of the heated length increases flow stability in forced circulation with a constant power density. However, change in heated length did not have any effect on the period of the oscillation (Boure et al, 1973).

1.3.5 Effect of non-uniform heat flux

Stability analysis of two-phase flow heated channels with symmetric and asymmetric axial heat-flux has been carried out by Rizwan-uddin (1994). It was found that different axial heat flux shapes result in varying stability predictions depending on several system parameters such as channel inlet subcooling.

The following chapter covers a brief literature review of analytical, numerical and experimental investigations performed to explore flow instability in natural circulation loops under supercritical conditions.

Chapter 2

Literature Survey

Future nuclear reactor designs are considering the possibility of operating with supercritical fluid to improve overall plant efficiency. Natural circulation core cooling is also an important feature of these new designs to promote passive safety of the systems that require stable natural-convection flow. Thus, it is necessary to accurately predict flow instability for flows with supercritical fluids, and design the systems to avoid flow instability. The basic objective of the present investigation is to explore flow instabilities of natural circulation loops with fluids under supercritical conditions.

To provide a comprehensive understanding, the available literature on stability of supercritical fluid flow in a single-channel, natural-convection loop is reviewed below. It is noted that due to relatively few applications, this topic has not attracted much attention in the past.

2.1 Analytical studies

An analytical model of supercritical flow in an idealized single-channel, natural-convection configuration (shown in Figure 2.1) to study system stability is developed by Chatoorgoon (2001). The system configuration is a constant cross-sectional area loop with constant boundary conditions for inlet temperature, inlet pressure and outlet pressure. To simplify the analysis and circumvent the high associated non-linearities, the heat source and sink ─ instead of being uniformly distributed along sides AB and CD ─ were assumed to be a point source and point sink configuration. It was postulated that the stability boundary for a single-channel, natural-circulation loop at supercritical conditions

can be approximated by the criterion $\frac{\partial(flow)}{\partial(power)} = 0$. This, in turn, yields the analytical expression for bounding power as a function of inlet conditions and loop geometry. The same point source and point sink configuration is also simulated using the SPORTS (Special Predictions Of Reactor Transients and Stability) code, and good agreement is reported in obtaining bounding power for stable flows (Chatoorgoon, 2001).

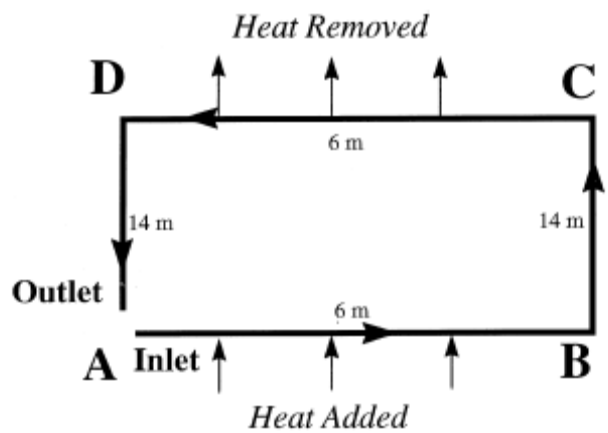

Figure 2.1: Schematic diagram of rectangular natural circulation loop (Chatoorgoon, 2001)

2.2 Numerical studies

Chatoorgoon (2001) also studied the supercritical flow stability phenomenon numerically for the same loop (shown in Figure 2.1) with distributed heat source and sink, using the SPORTS code (Chatoorgoon, 1986). In the SPORTS code, the general one-dimensional conservation equations are solved using a fully implicit numerical method. Moreover, property derivatives are avoided in the formulation of the numerical scheme to simplify the approach. The NIST property package is implemented as the state equation and called every time there is a need for state properties. It was found that the steady state profile of flow-rate versus power showed that the flow-rate initially increases with power, attains a maximum and then decreases with further power increase. It was suggested that the power corresponding to the maximum steady-state flow rate may be a good

approximation of the flow stability boundary. Flow instability is found by introducing a perturbation in the steady state inlet flow rate and then simulating a real-time transient. If the system is stable, the perturbation will decay with time and vanish, restoring the original steady-state solution. If the system is unstable, the perturbation will grow, precipitating flow oscillations, or a flow excursion, and the initial steady state will not be recovered (Chatoorgoon, 2001).

More recently, Chatoorgoon et al. (2005b and 2005c) reported an extended numerical study by examining effects of several different parameters on supercritical flow stability including inlet temperatures, inlet and outlet channel restriction coefficients (K factors), and different loop heights and heated lengths. In addition, this study also included effects of different fluids, like CO_2 and H_2. Based on the numerical results obtained it is concluded that stability characteristics of supercritical CO_2 are very similar to those of supercritical H_2O. Therefore, to fully explore the stability phenomenon, experimental studies may be performed more efficiently and economically using supercritical CO_2.

2.3 Experimental studies

There have been very few experimental studies of natural circulation with fluids near the critical point. Recently, experimental results of a natural circulation supercritical water (SCW) loop at University of Wisconsin-Madison is reported by Jain (2005). It is a vertical loop constructed from 2" diameter NPT Inconel 625 sch. 160 tubes to allow operation under supercritical conditions at 25 MPa pressure. The loop has two heaters installed on the lower horizontal section and on the left vertical leg, while two coolers are located along the upper horizontal section and the right vertical leg (see Figure 2.2). Molten lead is used as a heat transfer fluid in the heater and it surrounds the inner Inconel tube. Due to power input limitations, this SCW loop is tested for operating powers only up to 70 kW and was experimentally found to be stable (Jain, 2005).

Also, experiments were performed at Argonne National Laboratory (ANL) in a rectangular test loop with CO_2 — in place of water — to allow operation at moderate

temperature and pressure (Lomperski et al., 2004). The test loop consists of a lower horizontal heating section and an upper horizontal cooling section, connected by two vertical insulated pipes. All components of the loop are made of 316 type stainless steel. Heating is provided by a low voltage, high current AC power supply while two tube-in-tube heat exchangers are connected in parallel to provide cooling (see Figure 2.3). CO_2 is used, as it is a good substitute for water because of the analogous variation in thermophysical properties near the critical point. The test-loop was operated in the base configuration as well as with an orifice plate. No flow instabilities were observed in these tests *despite attempts to produce them with a variety of system perturbations* (Jain, 2005; Lomperski et al., 2004).

These experimental results deviate significantly from numerical predictions made by Jain (2005) and Chatoorgoon et al. (2005c). Detailed schematic diagrams of both test apparatus are shown in Figure 2.2 and Figure 2.3.

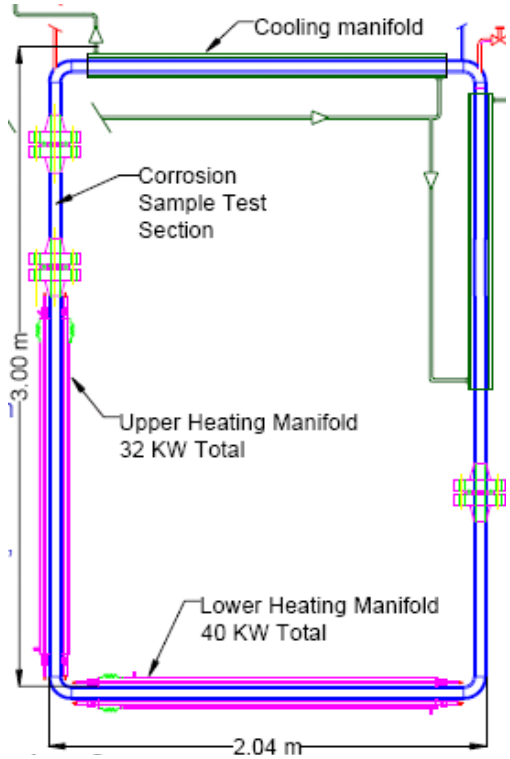

Figure 2.2: Schematic diagram of SCW test-loop at UW-Madison (Jain, 2005)

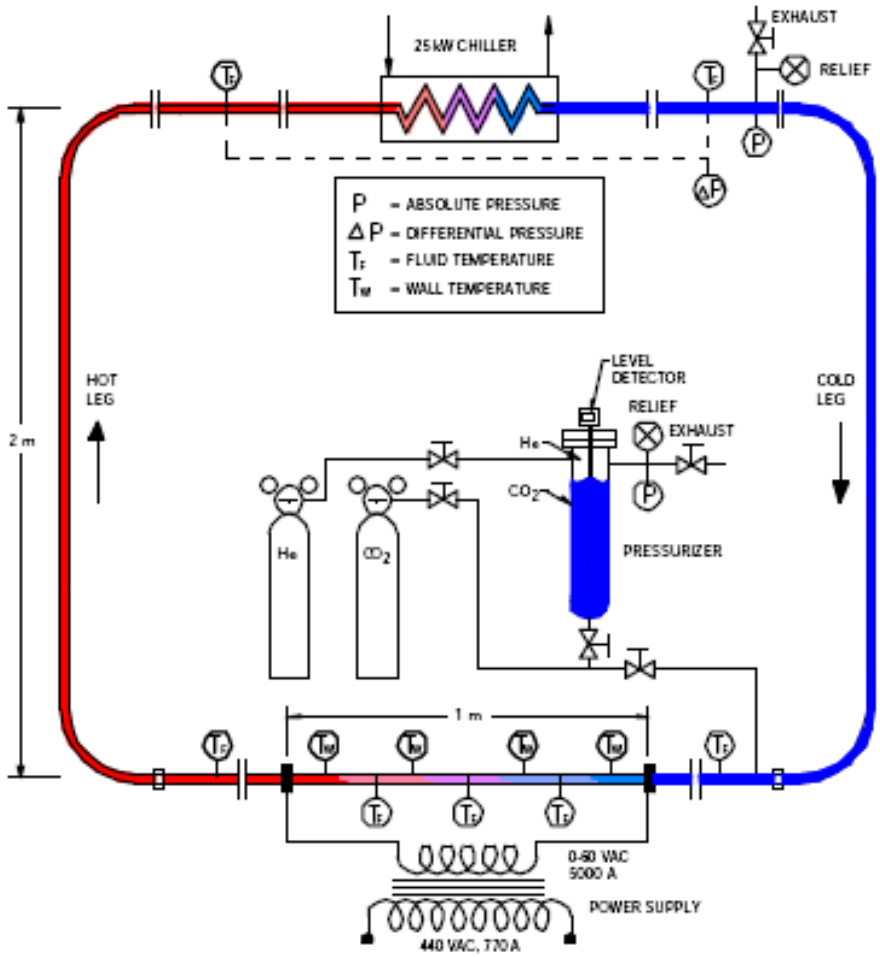

Figure 2.3: Schematic diagram of the CO_2 test loop at ANL (Lomperski et al., 2004; Jain, 2005)

Chapter 3

Model and Numerical Analysis

Flow stability is usually studied by solving the time-dependent conservation equations representing the system. These equations are generally solved either in frequency-domain or time-domain for the thermohydraulic stability analyses.

In the frequency-domain approach, these conservation equations along with the necessary constitutive laws are linearized about an operating point, Laplace transformed and then, stability predictions are made by applying classical control theory techniques. Moreover, system stability is analyzed with such well known methods as Bode plot, Nyquist plot, root-locus techniques, etc. Though very valuable, results of these frequency domain approaches are valid for infinitesimal perturbations only.

In the time-domain approach, time-dependent mass, momentum and energy conservation equations are solved numerically using finite-difference techniques. Usually, this approach is very time consuming when used for stability analyses, since the allowable time step size is very small, and large numbers of cases must be run to generate a stability map. However, with the advancement in computational resources, time domain investigation of flow stability has become a promising method compared with the other (frequency domain) standard approaches. It is usually performed to predict the threshold value of a system parameter (for example, heat flux or power level) below (or above) which the system is stable. The basic idea is to first solve the flow governing equations for the steady state and then treat the steady state solution as the initial condition for the transient flow. At time $t = 0$, a perturbation is introduced into the flow system. This perturbation can either be a fractional change in initial condition (which is actually the steady state solution) or a small change in the flow governing parameters (like heat flux, pressure boundary value, etc). Stability can also be investigated by momentarily

perturbing the steady state, for example, with a delta-function variation of a boundary condition. If the disturbance grows in time and yields sustained or diverging flow oscillations, then the steady-state system is considered to be unstable. On the other hand, if the disturbance leads to decaying oscillations resulting in convergence of flow and other field variables to the steady state solution, then the corresponding steady-state solution is considered to be stable.

Steady state and dynamic analyses of SCWR require appropriate modeling of the thermodynamic and transport properties of water near its critical point. Due to high nonlinearities associated, multi-dimensional modeling of the coolant channel becomes too complex. Therefore, for this preliminary investigation, a single-channel, one-dimensional model is developed. In this model, equations for the conservation of mass, momentum and energy are discretized using an implicit finite difference scheme. Thermophysical properties of the supercritical fluid are determined using the NIST property packages. Details of the model developed are described below.

3.1 Governing equations

3.1.1 Steady state equations

For one-dimensional channel flow, the steady state mass, momentum and energy conservation equations, and the equation of state can be written as follows:

<u>Continuity:</u>

$$\frac{\partial\left(\rho_{ss}u_{ss}\right)}{\partial z}=0 \tag{3.1}$$

<u>Momentum conservation:</u>

$$\frac{\partial\left(\rho_{ss}u_{ss}^{2}\right)}{\partial z}+\frac{\partial p_{ss}}{\partial z}+C_{k}\rho_{ss}u_{ss}^{2}+\rho_{ss}g\sin\theta=0 \tag{3.2}$$

Energy conservation:

$$\frac{\partial}{\partial z}\left[\rho_{ss}u_{ss}\left(h_{ss}+\frac{u_{ss}^2}{2}\right)\right]+\rho_{ss}u_{ss}g\sin\theta=q'''\tag{3.3}$$

State:

$$\rho_{ss}=eos\left(p_{ss},h_{ss}\right)\tag{3.4}$$

where: ρ_{ss}, u_{ss}, p_{ss} and h_{ss} are the fluid density, velocity, pressure and enthalpy, respectively, at steady state conditions. Also, g is the acceleration due to gravity, θ is the angle (anti-clockwise) of the flow direction from the horizontal plane, and q''' is the volumetric heat generation rate. Also, *eos* represents equation of state.

Coefficient C_k in the momentum conservation equation (3.2) is given by

$$C_k=\frac{f_{ss}}{2D_h}\tag{3.5}$$

where: D_h is the hydraulic diameter of the channel and f_{ss} is the friction factor, which can be obtained from the Blasius and McAdams relations (McAdams, 1954) for a smooth tube as:

$$f_{ss}=\begin{cases}0.316\,\mathrm{Re}_{ss}^{-0.25}, & \mathrm{Re}_{ss}<30{,}000\\ 0.184\,\mathrm{Re}_{ss}^{-0.20}, & 30{,}000<\mathrm{Re}_{ss}<10^6\end{cases}\tag{3.6}$$

where, Re_{ss} is the Reynolds number defined as

$$\mathrm{Re}_{ss}=\frac{\rho_{ss}u_{ss}D_h}{\mu_{ss}}\tag{3.7}$$

and μ_{ss} is the dynamic viscosity of the fluid in the channel. [‘ss’ in subscript represents steady state conditions]

3.1.2 Time dependent equations

For one-dimensional channel flow, the time-dependent mass, momentum and energy conservation equations, and the equation of state can be written as follows:

Continuity:

$$\frac{\partial \rho}{\partial t} + \frac{\partial (\rho u)}{\partial z} = 0 \tag{3.8}$$

Momentum conservation:

$$\frac{\partial (\rho u)}{\partial t} + \frac{\partial (\rho u^2)}{\partial z} + \frac{\partial p}{\partial z} + C_k \rho u^2 + \rho g \sin\theta = 0 \tag{3.9}$$

Energy conservation:

$$\frac{\partial}{\partial t}\left[\rho\left(h + \frac{u^2}{2}\right)\right] + \frac{\partial}{\partial z}\left[\rho u\left(h + \frac{u^2}{2}\right)\right] + \rho u g \sin\theta = \frac{\partial p}{\partial t} + q''' \tag{3.10}$$

State:

$$\rho = eos(p, h) \tag{3.11}$$

where: ρ, u, p and h are the fluid density, velocity, pressure and enthalpy, respectively.

Coefficient C_k in the momentum conservation equation (3.9) is given by

$$C_k = \frac{f}{2D_h} \tag{3.12}$$

where: D_h is the hydraulic diameter of the channel and f is the friction factor, which can be obtained from the Blasius and McAdams relations (McAdams, 1954) for a smooth tube as:

$$f = \begin{cases} 0.316\,\mathrm{Re}^{-0.25}, & \mathrm{Re} < 30{,}000 \\ 0.184\,\mathrm{Re}^{-0.20}, & 30{,}000 < \mathrm{Re} < 10^6 \end{cases} \tag{3.13}$$

where, Re is the Reynolds number defined as

$$\mathrm{Re} = \frac{\rho u D_h}{\mu} \tag{3.14}$$

and μ is the dynamic viscosity of the fluid in the channel.

The set of mass, momentum and energy conservation equations is closed by the equation of state for the supercritical fluid in the channel. In this study, supercritical properties of water and CO_2 are determined by employing NIST/STEAM 2.21 (Harvey et al., 2004) and NIST/REFPROP7 (Lemmon et. al., 2002), respectively. Further details about the NIST property packages and usage directions are given in Appendix B.

3.2 Spatial and temporal discretization

The governing equations, which form a system of non-linear equations, are solved numerically. Control-volume formulation techniques in space and forward-difference scheme in time, are employed to derive the finite difference equations for the mass, momentum and energy conservation.

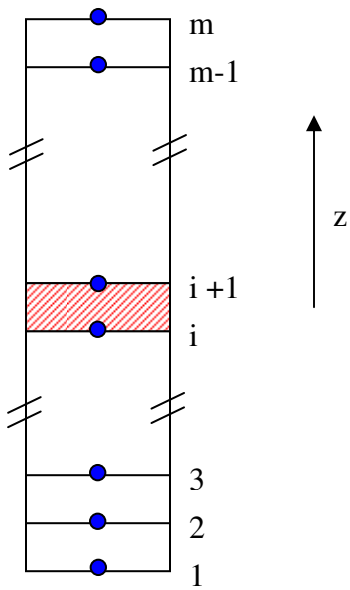

Figure 3.1: Spatial grid and control volume in the flow channel

The one-dimensional flow channel is divided into axial computational cells or control volumes, with the grid points located at the cell edges as shown in Figure 3.1. The first and last grid points of the domain coincide with the flow channel physical boundaries.

3.2.1 Steady state discretized equations

Integration of the steady state conservation equations (3.1) to (3.4) from grid point (i) to $(i+1)$ lead to the following discretized equations:

<u>Continuity:</u>

$$\left(u_{ss}\right)_{i+1} = \frac{(\rho_{ss} u_{ss})_i}{\left(\rho_{ss}\right)_{i+1}} \tag{3.15}$$

<u>Momentum conservation:</u>

$$\left(p_{ss}\right)_{i+1} = \left(p_{ss}\right)_i - \left(1 + \frac{1}{2}(C_k)_{i+1}\Delta z\right)(\rho_{ss} u_{ss}^2)_{i+1} + \left(1 - \frac{1}{2}(C_k)_i\,\Delta z\right)(\rho_{ss} u_{ss}^2)_i - \left(\frac{\left(\rho_{ss}\right)_i + \left(\rho_{ss}\right)_{i+1}}{2}\right) g\Delta z \sin\theta_i \tag{3.16}$$

<u>Energy conservation:</u>

$$\left(h_{ss}\right)_{i+1} = \frac{\left(\frac{q_i''' + q_{i+1}'''}{2}\right)\Delta z - \left(\frac{\left(\rho_{ss} u_{ss}\right)_{i+1} + \left(\rho_{ss} u_{ss}\right)_i}{2}\right) g\Delta z \sin\theta_i + \left(\rho_{ss} u_{ss} h_{ss}\right)_i}{\left(\rho_{ss} u_{ss}\right)_{i+1}} \tag{3.17}$$

<u>State:</u>

$$\left(\rho_{ss}\right)_{i+1} = eos\left(\left(p_{ss}\right)_{i+1}, \left(h_{ss}\right)_{i+1}\right) \tag{3.18}$$

where, the friction coefficient $(C_k)_i$ in equation (3.16) is defined by

$$(C_k)_i = \frac{f_{ss,i}}{2D_h} = \frac{1}{2D_h}\begin{cases} 0.316(\mathrm{Re}_{ss}^{-0.25})_i, & \mathrm{Re}_{\mathrm{ss,i}} < 30{,}000 \\ 0.184(\mathrm{Re}_{ss}^{-0.20})_i, & 30{,}000 < \mathrm{Re}_{\mathrm{ss,i}} < 10^6 \end{cases} \tag{3.19}$$

and $\mathrm{Re}_{ss,i}$ is given by

$$\mathrm{Re}_{ss,i} = \frac{(\rho_{ss} u_{ss})_i}{\mu_{ss,i}} D_h \tag{3.20}$$

3.2.2 Time dependent discretized equations

Integration of the time dependent conservation equations (3.8) to (3.11) from grid point (i) to $(i+1)$ and forward difference approximation for the time derivative yield the following set of implicit discretized equations:

<u>Continuity:</u>

$$u_{i+1}^{n+1} = \frac{(\rho u)_i^{n+1} - \eta\left(\rho_i^{n+1} - \rho_i^n + \rho_{i+1}^{n+1} - \rho_{i+1}^n\right)}{\rho_{i+1}^{n+1}} \tag{3.21}$$

<u>Momentum conservation:</u>

$$\begin{aligned} p_{i+1}^{n+1} = p_i^{n+1} &- \left(1 + \frac{1}{2}(C_k)_{i+1}^n \Delta z\right)(\rho u^2)_{i+1}^n + \left(1 - \frac{1}{2}(C_k)_i^n \Delta z\right)(\rho u^2)_i^n - \left(\frac{\rho_i^n + \rho_{i+1}^n}{2}\right) g \Delta z \sin\theta_i \\ &+ \eta\left((\rho u)_i^{n+1} - (\rho u)_i^n + (\rho u)_{i+1}^{n+1} - (\rho u)_{i+1}^n\right) \end{aligned} \tag{3.22}$$

<u>Energy conservation:</u>

$$h_{i+1}^{n+1} = \frac{\left(\frac{q_i''' + q_{i+1}'''}{2}\right)\Delta z - \left(\frac{(\rho u)_{i+1}^{n+1} + (\rho u)_i^{n+1}}{2}\right) g \Delta z \sin\theta_i - \eta\left\{(\rho h)_i^{n+1} - (\rho h)_{i+1}^n - (\rho h)_i^n\right\} + (\rho u h)_i^{n+1}}{(\rho u)_{i+1}^{n+1} + \eta \rho_{i+1}^{n+1}} \tag{3.23}$$

<u>State:</u>

$$\rho_{i+1}^{n+1} = eos\left(p_{i+1}^{n+1}, h_{i+1}^{n+1}\right) \tag{3.24}$$

where the friction coefficient $(C_k)_i^n$ in equation (3.22) is defined by

$$(C_k)_i^n = \frac{f_i^n}{2D_h} = \frac{1}{2D_h}\begin{cases} 0.316(\mathrm{Re}^{-0.25})_i^n, & \mathrm{Re}_i^n < 30{,}000 \\ 0.184(\mathrm{Re}^{-0.20})_i^n, & 30{,}000 < \mathrm{Re}_i^n < 10^6 \end{cases} \tag{3.25}$$

and Re_i^n is given by

$$\mathrm{Re}_i^n = \frac{(\rho u)_i^n}{\mu_i^n} D_h \tag{3.26}$$

In the above set of discrete equations, η is given by $\frac{\Delta z}{2\Delta t}$ where Δz and Δt correspond to the spatial grid size and time step, respectively.

In deriving the finite difference equations, the effect of integrating across a computational cell is analogous to averaging the field and flow variables in that cell, and leads to better accuracy compared to the first order difference scheme of the spatial derivatives.

3.3 Boundary conditions

Solution of the system of non-linear governing equations depends upon the choice of boundary conditions. For the present investigation, constant pressure drop boundary condition along with constant inlet conditions are applied to the flow channel, i.e. inlet temperature, inlet pressure and outlet pressure are known.

For the case of zero total pressure drop (natural circulation) inside the flow channel, these boundary conditions may be physically achieved by connecting both ends of the channel to a large reservoir, in which constant inlet conditions are maintained (Chatoorgoon, 2001; Chatoorgoon et al., 2005b,c; Jain, 2005).

3.4 Solution algorithm

3.4.1 Steady state solution algorithm

Details of the solution algorithm employed to solve the coupled, nonlinear, steady state equations, (3.15) to (3.18) are given below (Chatoorgoon, 1986):

There are four unknown variables (ρ_{ss} , u_{ss} , p_{ss} and h_{ss}) to be solved for each grid point i .

1) Inlet conditions of the flow channel are maintained constant, therefore, at grid point 1:

$$(\rho_{ss})_1 = \rho_{\text{in}} = \text{constant}$$

$$(p_{ss})_1 = p_{\text{in}} = \text{constant}$$

$$(h_{ss})_1 = h_{in} = \text{constant}$$

2) Velocity at the channel inlet $(u_{ss})_1$, is guessed initially.

3) Following steps (a) and (b) are repeated for i = 1,…, (m-1)

   a) A value for $(\rho_{ss})_{i+1}$ is guessed at the $(i+1)^{th}$ grid point.

   b) All the variables on the RHS of the steady state continuity equation (3.15) are now known. Using this equation, velocity $(u_{ss})_{i+1}$ is calculated. This, in turn, yields solution for $(p_{ss})_{i+1}$ and $(h_{ss})_{i+1}$ from equations (3.16) and (3.17), respectively. Now, using this pressure and enthalpy values, state equation (3.18) is solved for density $(\tilde{\rho}_{ss})_{i+1}$. This step (b) is repeated (until a desired convergence is reached) with this updated density value $(\tilde{\rho}_{ss})_{i+1}$ serving as a guess for $(\rho_{ss})_{i+1}$.

4) At convergence, all the unknown variables at each grid point are calculated up to the outlet of the flow channel including a value for $(p_{ss})_m$, where a constant exit pressure, p_{out} , is specified as boundary condition.

5) Calculated pressure at the outlet, $(p_{ss})_m$, is compared with the constant specified pressure p_{out}. If the difference $\left|p_{out} - (p_{ss})_m\right|$ is within the specified tolerance limit, then the simulation terminates. Otherwise, step (3) is repeated with <u>another</u> guess value for $(u_{ss})_1$ until the pressure boundary condition at the exit (grid m) is satisfied within specified tolerance. Improved guess for $(u_{ss})_1$ can be obtained by employing either the "Bisection method" or the "Regula-Falsi method". [Not surprisingly, Regula-Falsi method leads to faster convergence than the Bi-section method.]

3.4.2 Time dependent solution algorithm

Details of the solution algorithm employed to solve the coupled, nonlinear, time dependent equations, (3.21) to (3.24) are given below (Chatoorgoon, 1986):

There are four unknown variables (ρ, u, p and h) to be solved for each grid point i.

I. <u>Initial condition</u>: At $t = 0$, all unknown variables are assumed to be known for each grid point i.

$$\rho_i^0 = \text{known}$$

$$u_i^0 = \text{known}$$

$$p_i^0 = \text{known}$$

$$h_i^0 = \text{known}$$

II. <u>Boundary conditions</u>: As inlet conditions of the flow channel are maintained constant, for each $(n+1)^{th}$ time step, at grid point 1

$$\rho_1^{n+1} = \rho_{\text{in}} = \text{constant}$$

$$p_1^{n+1} = p_{\text{in}} = \text{constant}$$

$$h_1^{n+1} = h_{in} = \text{constant}$$

III. For the $(n+1)^{th}$ time step,

a) Velocity at the channel inlet u_1^{n+1}, is guessed

b) Following two steps (b.1 and b.2) are repeated for i = 1,…, (m-1)

b.1) A value for ρ_{i+1}^{n+1} is guessed at the $(i+1)^{th}$ grid point.

b.2) All the variables on the RHS of the time dependent continuity equation (3.21) are now known. Using this equation, velocity u_{i+1}^{n+1} is calculated. This, in turn, yields solution for p_{i+1}^{n+1} and h_{i+1}^{n+1} from equations (3.22) and (3.23), respectively. Now, using this pressure and enthalpy values, state equation (3.24) is solved for density $\tilde{\rho}_{i+1}^{n+1}$. This step (b.2) is repeated (until a desired convergence is reached) with the updated density value $\tilde{\rho}_{i+1}^{n+1}$ serving as a guess for ρ_{i+1}^{n+1}.

c) At convergence, all the unknown variables at each grid point are calculated up to the outlet of the flow channel, where a constant exit pressure, p_{out}, is specified.

d) Calculated pressure at the outlet, p_m^{n+1}, is compared with the constant specified pressure p_{out}. If the difference $\left|p_{out} - p_m^{n+1}\right|$ is within the specified tolerance limit, then simulation moves to the next time step level. Otherwise, step IIIb is repeated with <u>another</u> guess value for u_1^{n+1} (in step IIIa) until the pressure boundary condition at the exit (grid m) is satisfied within the specified tolerance. Improved guess for u_1^{n+1} can be obtained by employing either the "Bisection method" or the "Regula-Falsi method".

Numerical scheme and algorithm described above are used in the next chapter to simulate supercritical water and CO_2 loops and to study their stability characteristics.

Chapter 4
FIASCO Code Validation

A computer code called FIASCO (Flow Instability Analysis under SuperCritical Operating conditions) is developed in FORTRAN90 to simulate the dynamics of a natural circulation loop with supercritical fluid. For the validation of the code, as well as to gain some insight into the dynamics of the natural circulation mechanism under supercritical conditions, several results available in the literature were reproduced using this code. Details of some of the numerical verification exercises are described in the following sections.

4.1 ANL CO_2 Loop

A numerical model and a computer code were developed by Lomperski et al. (2004) to simulate the stability of the CO_2 natural circulation loop at ANL (see Figure 2.3). They also presented numerical results for the steady-state mass flux as a function of input power as well as heater outlet temperature for the given inlet conditions. These results along with the results of their stability simulations (for the base loop configuration, i.e. with no flow obstructions) are reproduced successfully using the FIASCO code, verifying the accuracy of the model and numerical scheme used. Figures 4.1 to 4.3 compare numerical results obtained using the FIASCO code with the results reported by Lomperski et al. (2004). At steady state, experimentally measured bulk fluid temperature at the heater outlet and the calculation results by Jain (2005) are plotted against input power in Figure 4.1(a). FIASCO simulated results for the same configuration are shown in Figure 4.1(b). Due to unavailability of appropriate friction factor data for the experiments performed at ANL, the friction factor correlation in FIASCO code is varied (in this case, C_k is increased by a factor of 4) in order to match the heater outlet

temperature within a certain tolerance. Computed results for steady state mass flux, shown in Figure 4.2(b), indicate good agreement with both the experimental results as well as numerical predictions by Lomperski et al. (2004) shown in Figure 4.2(a).

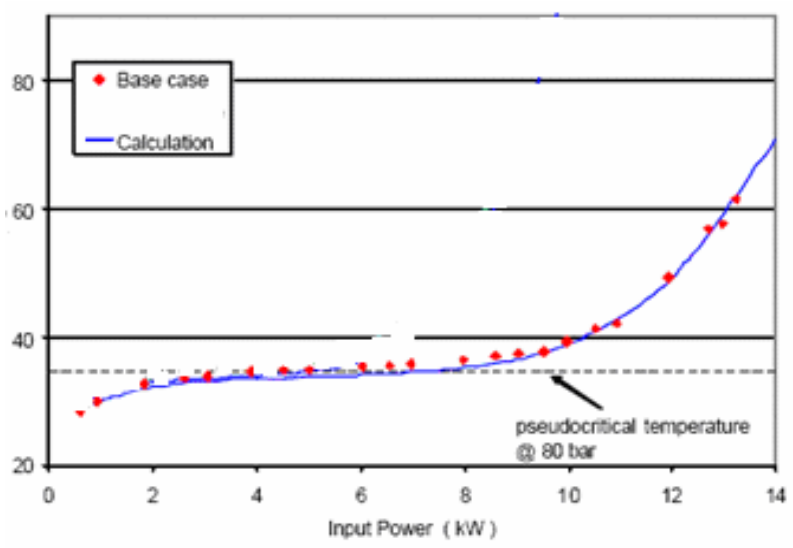

(a)

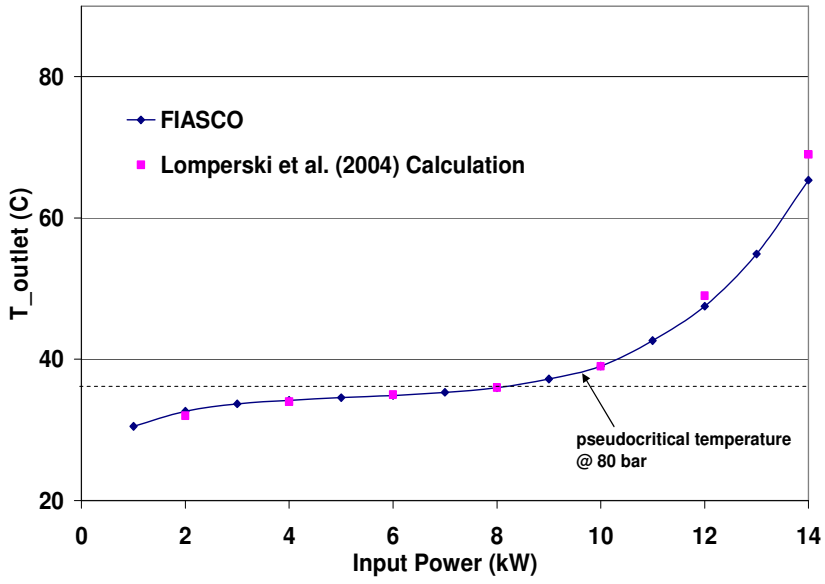

(b)

Figure 4.1: Heater outlet temperature for the base case at $P_{in} = P_{out} = 80$ bar and $T_{in} = 24$ C (a) Lomperski et al. (2004); (b) FIASCO

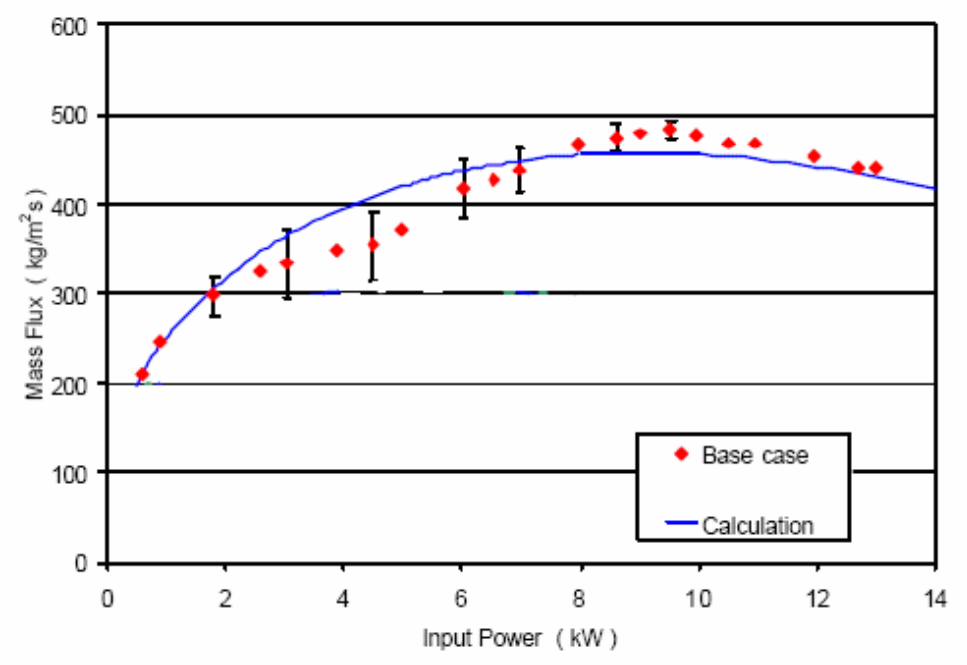

(a)

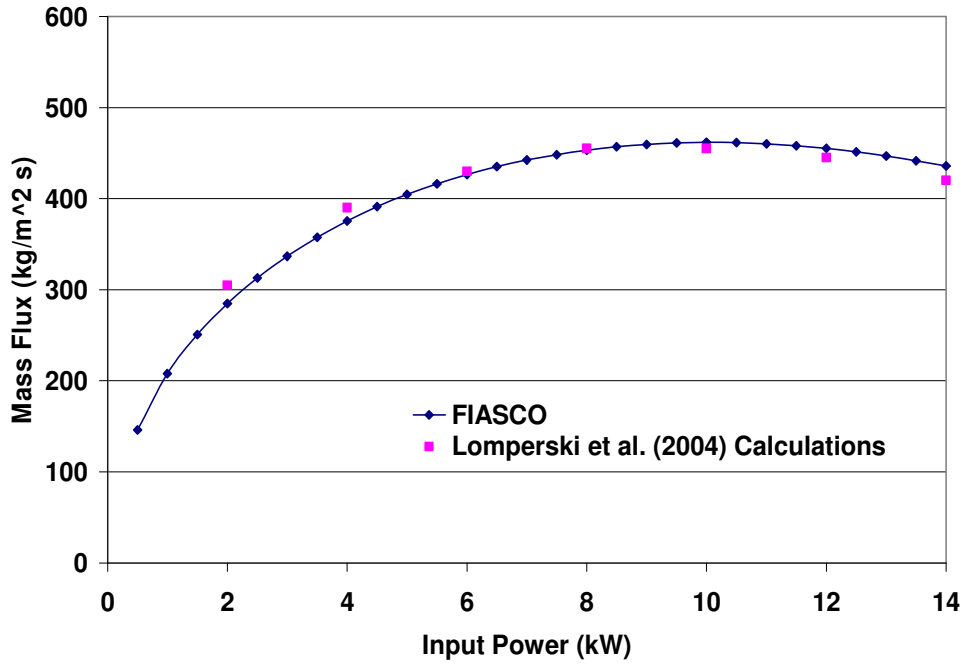

(b)

Figure 4.2: Steady state mass flux at 80 bar and T_{inlet} = 24 C (a) Lomperski et al. (2004); (b) FIASCO

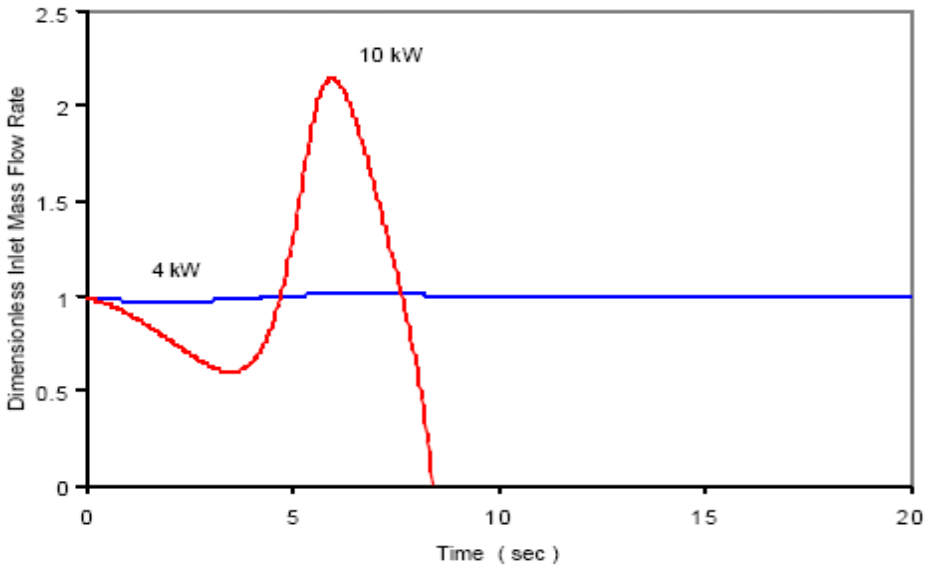

(a)

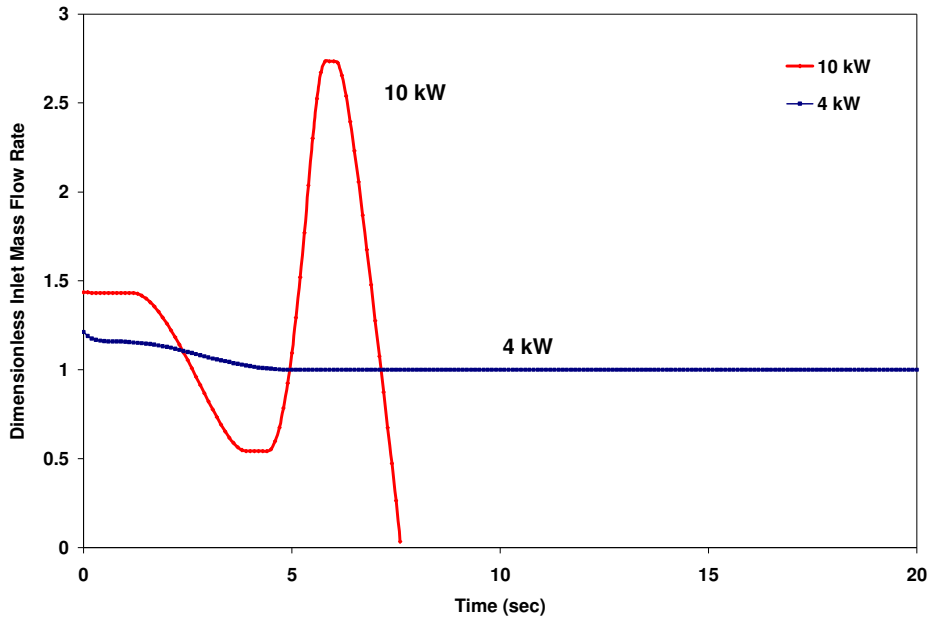

(b)

Figure 4.3: Inlet mass flow rate in response to a perturbation at t = 0 for base loop configuration (a) Lomperski et al. (2004); (b) FIASCO

Effect of two power levels on system stability as simulated using the FIASCO code and compared with the results reported in Lomperski et al. (2004) is shown in Figure 4.3. In this figure, mass flux is normalized with the corresponding steady state value. Results

obtained using the FIASCO code agree well with the results presented in Lomperski et al. (2004). However, slight discrepancy in the quantitative results may be due to the difference in type of perturbation applied. FIASCO results, shown in Figure 4.3(b), are obtained using an initial condition in which the velocity along the whole channel is increased by 20 % from the corresponding value at the steady state. Perturbation in Lomperski et al. is of 0.1 kW change in heating power at t = 0. All other field variables at t = 0 are kept at their steady state values.

4.2 Simplified Water Loop

Steady state results were reported in Jain (2005) for a simplified natural circulation loop geometry shown in Figure 4.4. This geometry is based on the loop configuration analyzed in Chatoorgoon et al. (2005b). Results reported include effect of inlet temperatures (ranging from 600 K to 655 K) on the variation of steady state mass flow rate with power and are shown in Figure 4.5(a). These results are compared with those obtained using the FIASCO code in Figure 4.5(b). Reasonably good agreement is achieved.

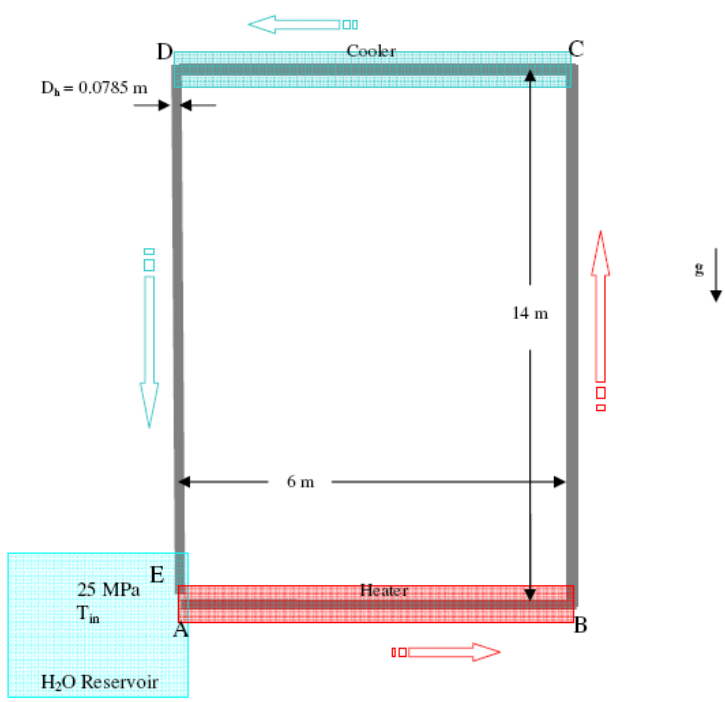

Figure 4.4: Schematic diagram of Simplified Water Loop

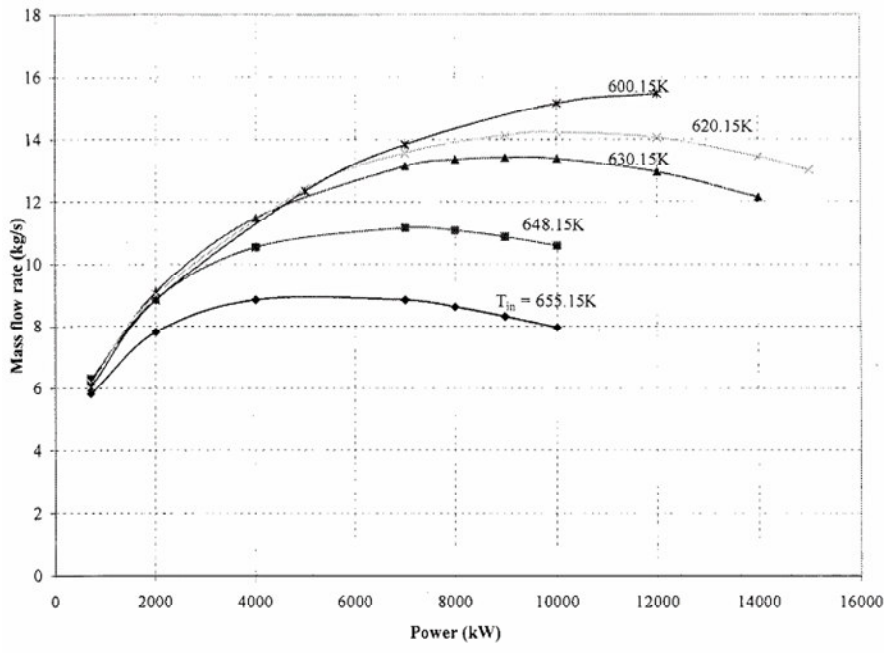

(a)

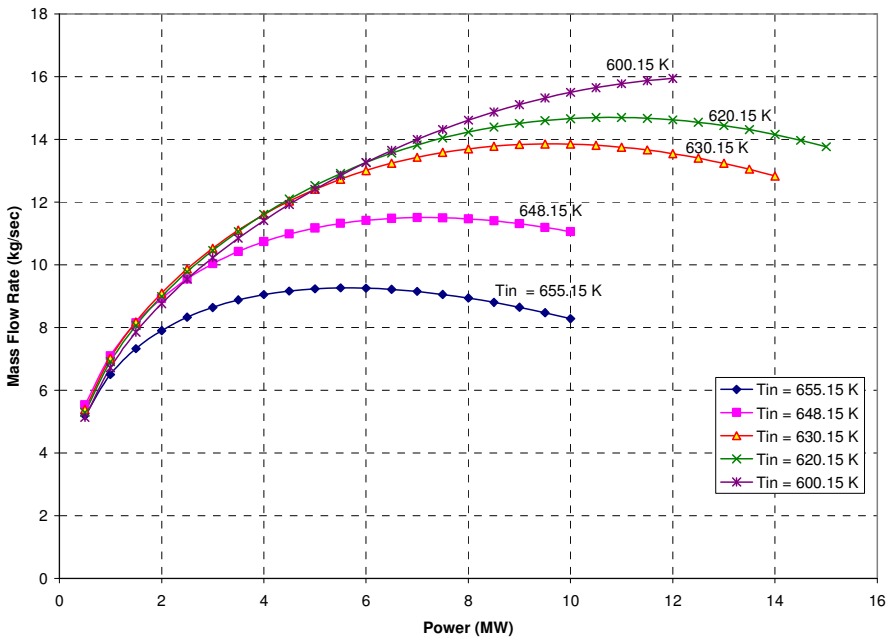

(b)

Figure 4.5: Steady state mass flow rate versus power curve for Simplified Water Loop (a) Jain (2005); (b) FIASCO

From these comparison exercises, it is apparent that FIASCO simulated results for the ANL CO_2 loop and Simplified Water Loop yield good agreement with the results available in the literature and hence provides confidence in the ability of the FIASCO code to simulate additional scenarios and in more complex geometries.

After the testing and verification exercise, the task of a systematic steady state and stability analysis of a natural circulation supercritical fluid loop was undertaken. In this context, parametric studies for a simple rectangular loop were performed in detail to analyze the effect of different geometries as well as flow parameters on stability. Moreover, to gain a better understanding of the dynamics of the rectangular supercritical natural circulation loop, a simplified geometry was chosen and detailed numerical study was performed to predict the stability boundary of such a flow system.

Chapter 5

Stability Analysis of a CO_2 Loop

5.1 Model of the CO_2 Loop

For the time domain stability analysis and parametric studies, a simple single-channel rectangular loop (same as in Chatoorgoon et al. (2005c)) is chosen. A schematic diagram and geometric parameters for the loop are shown in Figure 5.1. It is essentially a constant area loop with lower horizontal heating and upper horizontal cooling sections. Heat source and sink are assumed to be of equal magnitude, and uniformly distributed along the respective sections. Also, energy is assumed to be directly deposited to or extracted from the respective sections eliminating the need to model wall heat transfer mechanisms. Both, inlet and outlet of the loop are assumed to be connected to a large reservoir or pressurizer chamber in order to maintain constant inlet conditions (i.e. constant pressure and temperature at point A) during the operation of the loop. Also, a zero total pressure drop boundary condition is applied in the flow loop, which in turn gives another boundary condition at the outlet point, O.

The stability analysis is performed with supercritical carbon dioxide as the working fluid. [CO_2 is often used in supercritical fluid experiments due to its viability and similarity in thermo-physical properties' variations compared to water at supercritical conditions. Moreover, due to lower critical pressure for CO_2, conducting physical experiments are less demanding on safety, power etc.] Reservoir conditions are maintained at 25 C temperature and 8 MPa pressure, which provide inlet pressure, inlet temperature and outlet pressure boundary conditions for the flow loop. Moreover, inlet and exit restriction

loss coefficients — R_{k_1} = 0.5 and R_{k_2} = 0.5, respectively, — are included, by modifying C_k as, $C_{k_i} = \frac{f_i}{2D_h} + \frac{R_{k_i}}{\Delta z}$ for the inlet and outlet grid points.

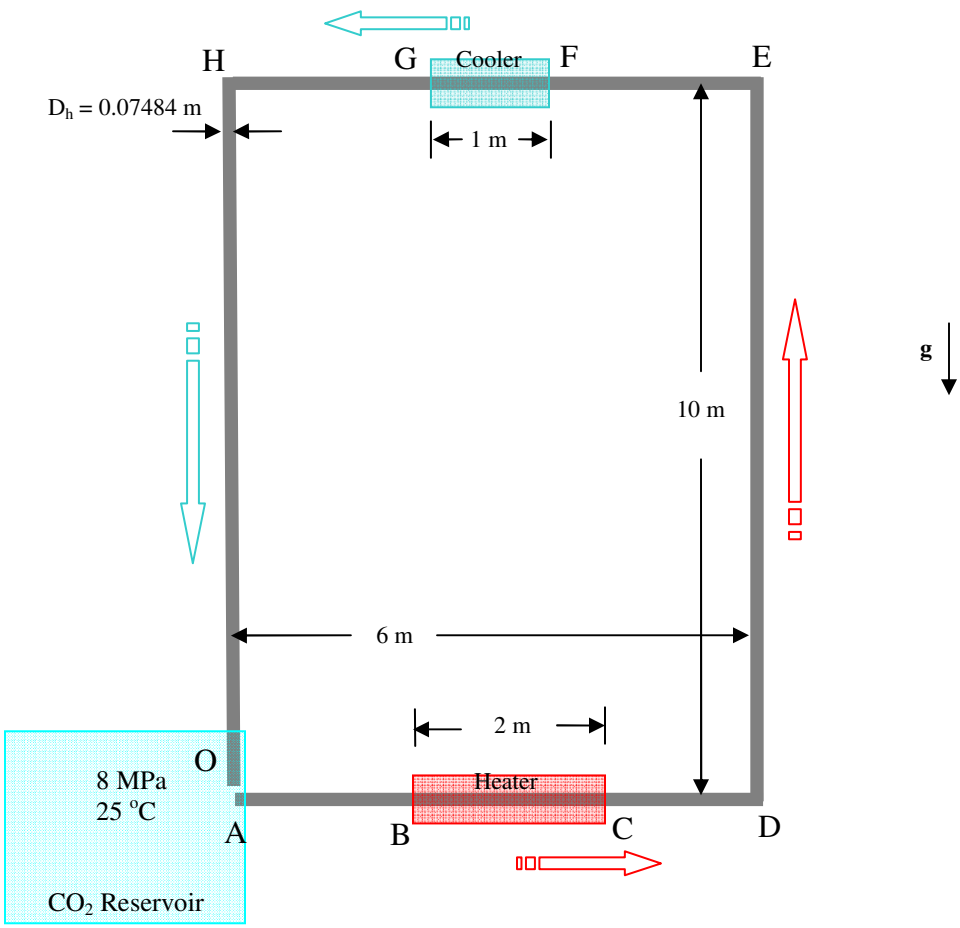

Figure 5.1: Schematic diagram of the flow loop

For given parameter values, the steady-state solution is determined first by employing the numerical approach described in Chapter 3. The NIST REFPROP7 package (Lemmon et al., 2002) is modified and linked to the FORTRAN code. It is used as the state equation to provide thermo-physical properties data for CO_2. The steady-state solution for the unknown variables (ρ, u, p and h) is used as an initial condition at every grid point for the transient simulations. It is noted here that perturbations can be introduced in any

of the unknown variables by disturbing its steady state values fractionally. For the analysis presented here, steady state velocities are perturbed (positively) by 1 % and used as an initial condition for velocity at each grid point. Then, at every time step, discrete variables are evaluated throughout the domain with the exit pressure boundary condition satisfied within the tolerance limit of 10^{-6} MPa. If, the perturbation grows in time, i.e. inlet velocity (and velocity at all grid points) oscillations diverge as time increases, then the system is considered to be unstable. Otherwise, if the perturbation decays in time, i.e. inlet velocity oscillations dampen and inlet velocity returns to its steady state value, then the system is considered to be stable. Power level at which flow oscillations nearly sustain their amplitude (i.e. neither diverge nor converge), is called the threshold power (stability boundary) for that flow system.

5.2 Steady state analysis

The steady-state solution is determined by solving the steady state governing equations for the one-dimensional flow channel. Steady-state behavior of the natural circulation loop with supercritical fluid is simulated at different power levels while maintaining the inlet condition constant. The results in Figure 5.2 (a), obtained with a grid size of Δx = 0.1 m, show that the steady-state flow rate initially increases with power, reaches a maximum at about 2 MW and then decreases. While comparing steady-state results obtained using the FIASCO code with those obtained using the SPORTS code (shown in Figure 5.2 (b)), it is observed that the two flow-power curves match fairly well for low values of power. However, there exists some discrepancy in the after-peak region. A mesh sensitivity study is also performed to observe the effects of spatial grid size on the steady state flow-power curve, and is shown in Figure 5.3. It is observed that results do change slightly with mesh refinement; however, there is no significant effect on flow stability, as explained in sections below. Therefore, spatial grid size of 0.1 m was chosen in subsequent steady state and transient simulations in order to optimize the computational load.

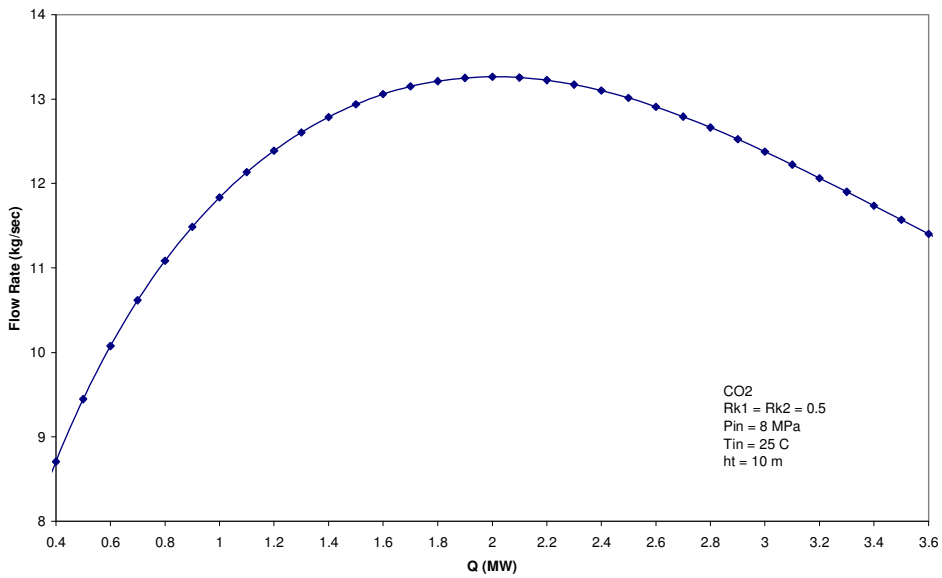

(a)

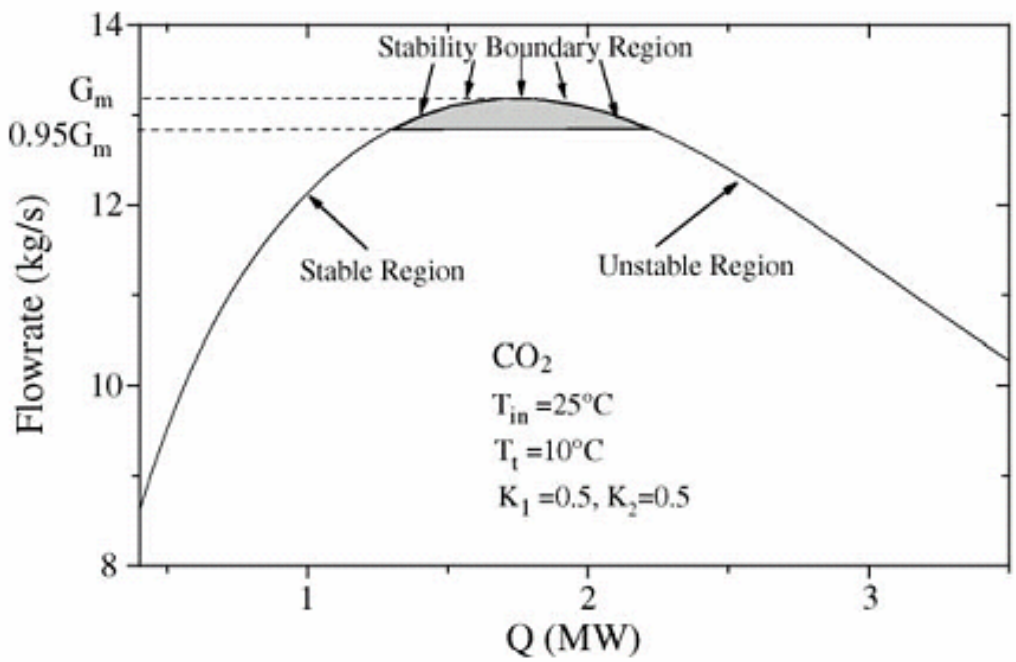

(b)

Figure 5.2: Steady state flow rate profile for CO_2 (with 0.1 m grid size); (a) FIASCO (b) Chatoorgoon et al. (2005)

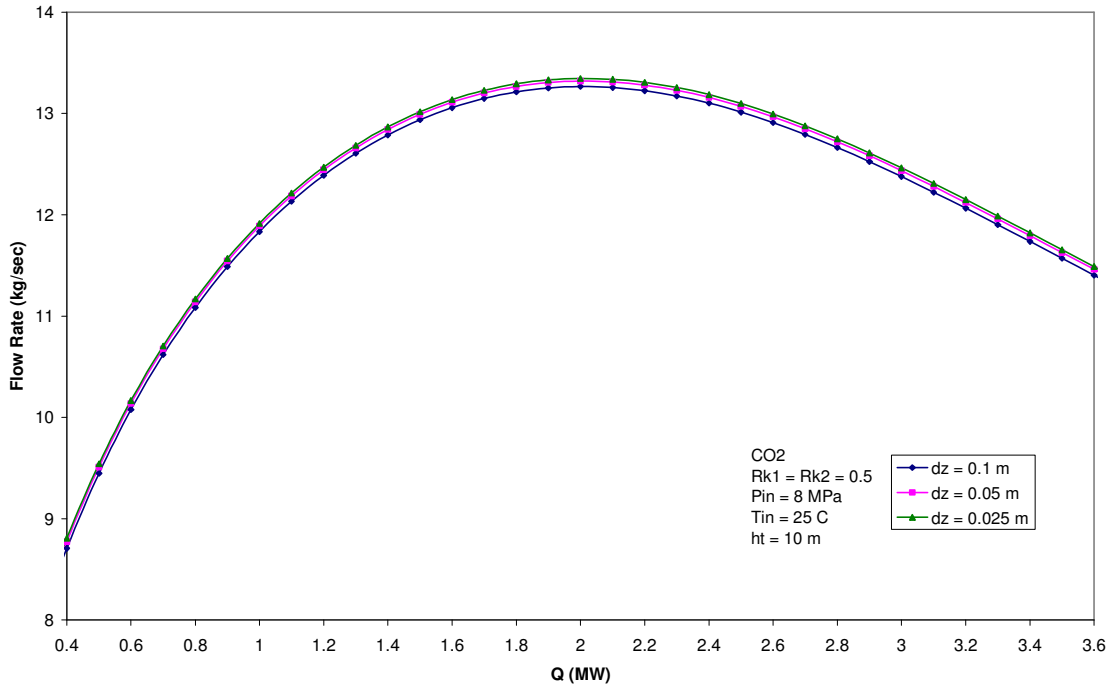

Figure 5.3: Effect of spatial mesh refinement on the steady state results

5.3 Numerical tests

The initial round of transient analyses with the FIASCO code is carried out with a spatial grid size of 0.1 m and time step size of 0.35 sec (same as in Chatoorgoon et al., 2005c). Flow is perturbed at each steady state, and the growth or decay of perturbation over time indicates whether the system at this steady state is unstable or stable, respectively. Inlet velocity evolution for three different power levels is shown in Figure 5.4. From the results shown in Figure 5.4, it is clear that flow oscillations at 1.50 MW decay, i.e. the system is stable, and the flow oscillations at 1.53 MW grow, i.e. the system is unstable, and hence the power threshold for stability for this system is between $1.50 < P < 1.53$ MW. This is in good agreement with the results reported in Chatoorgoon et al. (2005c) for the same spatial grid size and time step and shown in Figure 5.2 (b).

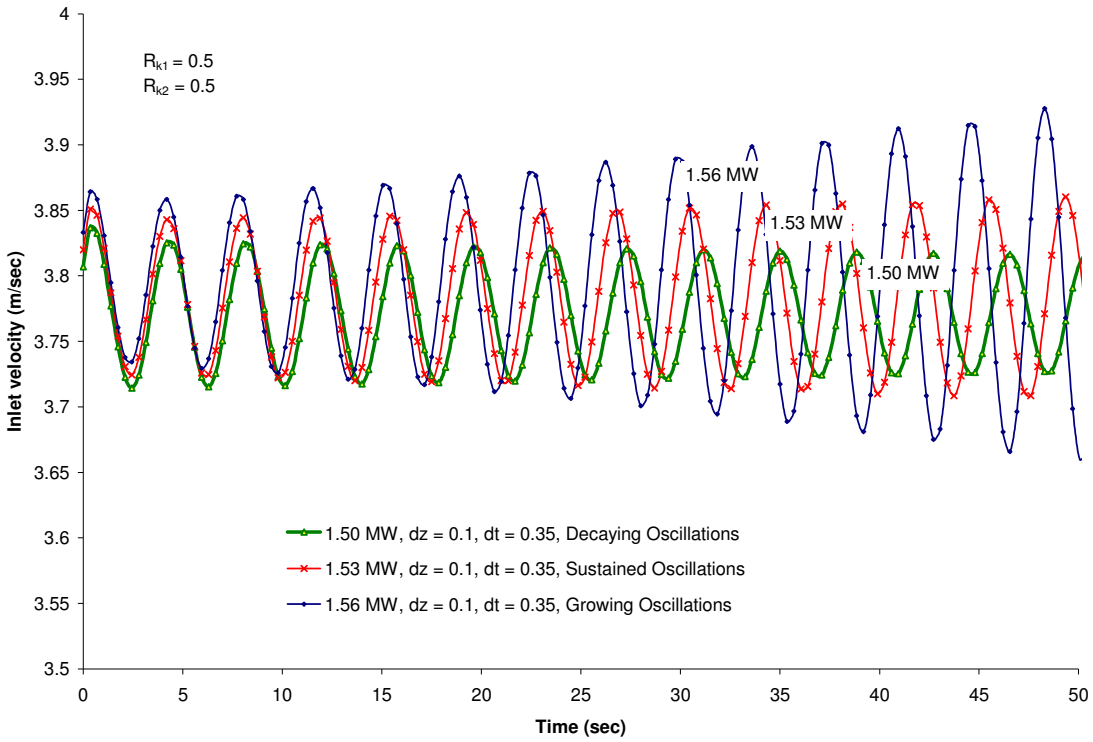

Figure 5.4: Inlet velocity as a function of time for three different power levels. The stability boundary is between 1.50 MW and 1.53 MW (with Δz = 0.1 m and Δt = 0.35 sec)

In an attempt to reproduce the results reported by previous investigators, results presented in Figure 5.4 were obtained with Δz = 0.1 m and Δt = 0.35 sec. However, to ensure temporal and spatial grid independence of the results, a grid refinement study is performed and the results, presented in the sections below, show that the stability threshold does in fact change as spatial and temporal steps are refined.

5.3.1 Effect of temporal grid refinement

For the temporal grid refinement study, 1 MW power, that is well below the stability boundary of ~ 1.53 MW, is chosen, and the system is predicted to be highly stable for the spatial grid size of 0.1 m and the time step size of 0.35 sec. As shown in Figure 5.5, further reducing the time step to half and quarter values produces sustained and growing

flow oscillations, respectively. This shows the high sensitivity of the numerical approach on the time step size. It is deduced that a large time step induces numerical diffusion and hence (artificial) flow stability into the system. Therefore, it is concluded that $\Delta t = 0.35$ sec is most likely too large a time step for accurate stability analysis. Further reductions of the time step yield the time-step size independent converged solution for 0.021875 (0.35/16) sec time step, as shown in Figure 5.6.

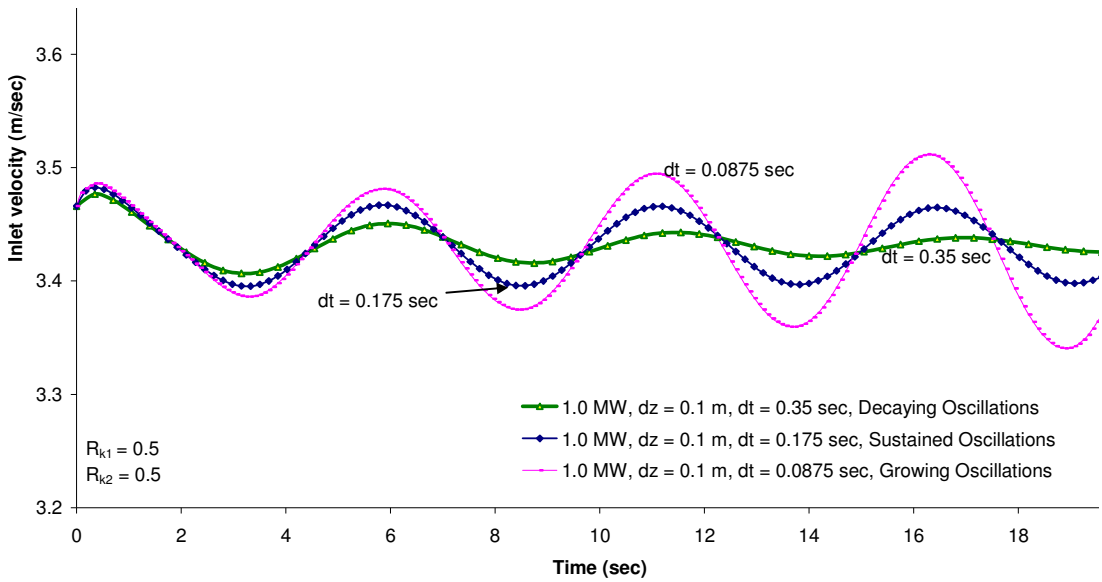

Figure 5.5: Effect of reducing time step on the transient solution at 1.0 MW

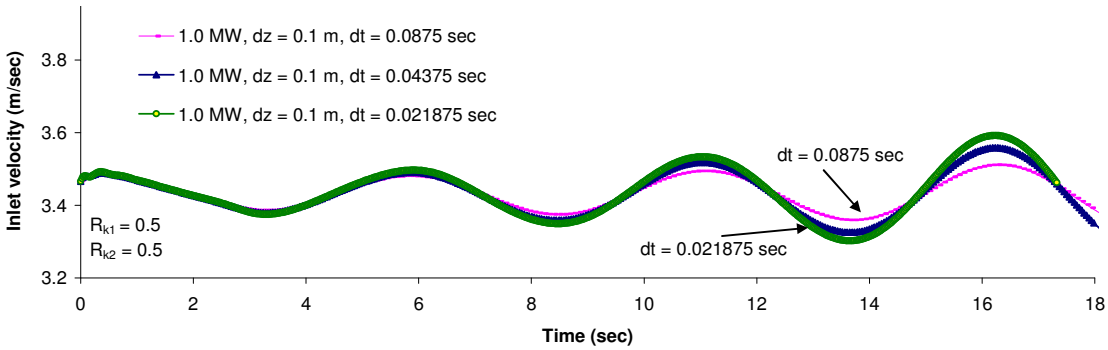

Figure 5.6: Further time step refinement at 1.0 MW

It should be noted that though temporal grid refinement steps are not reported by Jain (2005), results presented in that reference are obtained with time steps closer to 0.02 sec.

5.3.2 Effect of spatial grid refinement

To ensure the convergence of the numerical solution, a spatial grid refinement study is also performed. Effects of different grid size on the numerical solution are shown in Figures 5.7 and 5.8 for 1.0 MW and 0.7 MW power, respectively.

In Figure 5.7, temporal variation in inlet velocity is presented for different spatial grid sizes at 1.0 MW power. Note that the time step used for results in this figure is 0.35 sec. [Though the system is seen to be stable for this time step, as shown in Figure 5.7, the system is actually unstable at smaller time step values.] It can be seen that reducing the spatial grid size does not have a significant effect on system stability, as the system remains stable at finer spatial resolutions producing spatially converged results. Though a shift in oscillations is observed, the magnitude and frequency of oscillations remain the same.

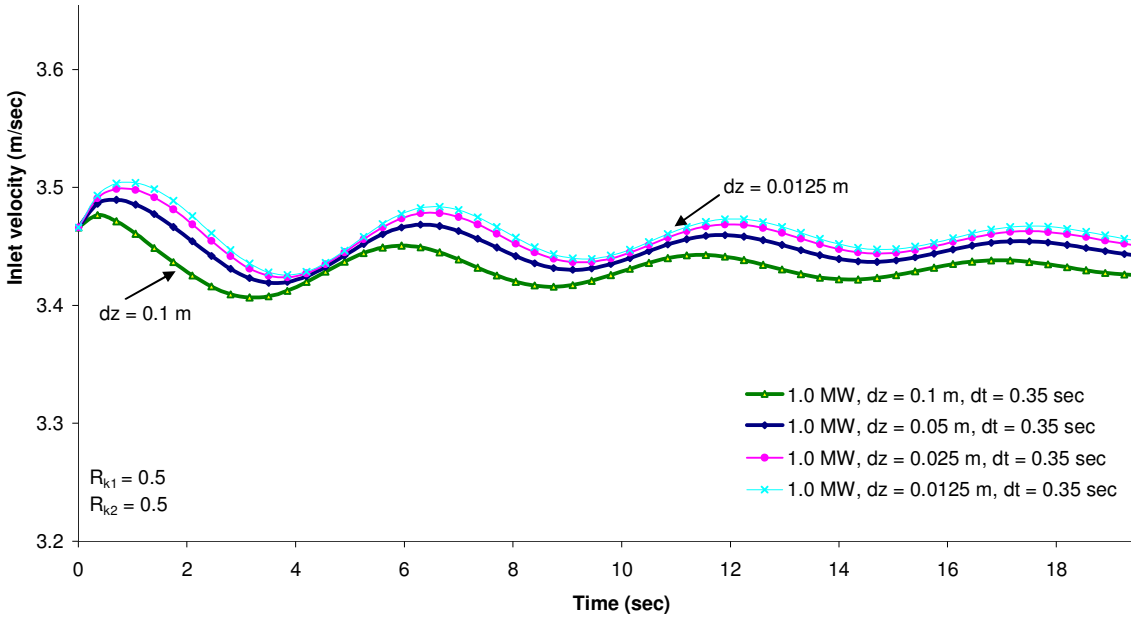

Figure 5.7: Effect of reducing spatial grid size on the transient solution at 1.0 MW

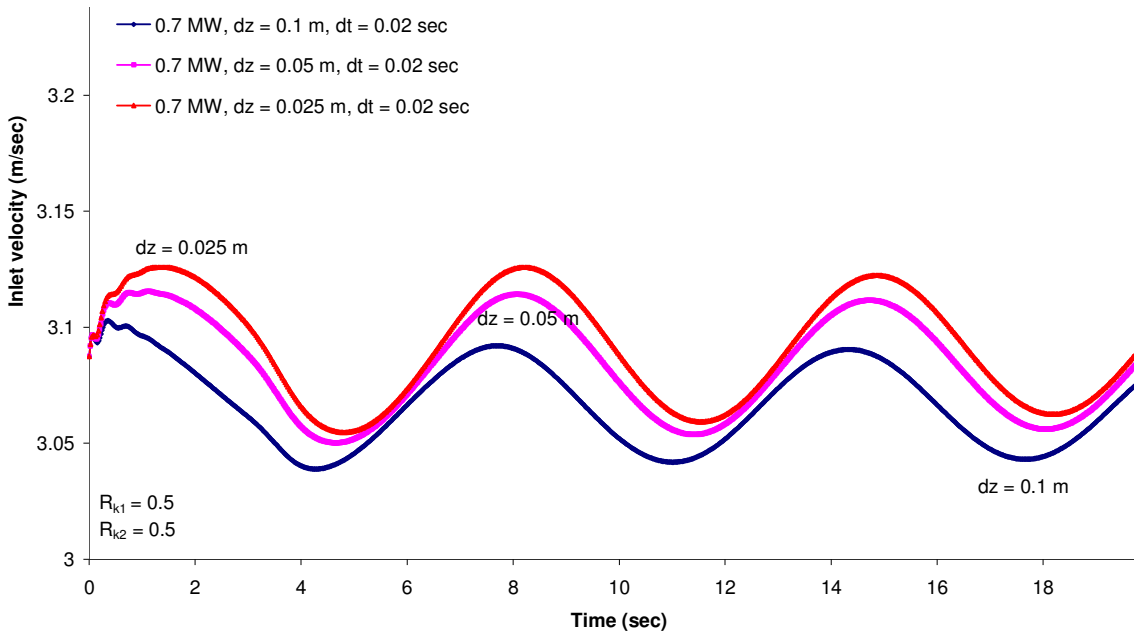

Figure 5.8: Effect of reducing spatial grid size on the transient solution at 0.7 MW

Furthermore, to predict the effect of spatial grid resolution on an *actually* stable system, a grid refinement study is performed at 0.7 MW power level and results obtained using $\Delta t = 0.02$ sec are presented in Figure 5.8. Once again, it is clear that a nearly stable system remains so as Δz is refined, suggesting that $\Delta z = 0.1$ m is adequate for the stability analysis of this system.

5.3.3 Effect of stringent pressure boundary tolerance

In order to accurately predict the stability boundary of the system, it is noted that the pressure boundary condition at the outlet of the channel should be strictly satisfied. Otherwise, the results could be misleading. The effect of different tolerances allowed in the imposition of pressure boundary conditions at the exit (parameter pb) on the numerical evaluation of system stability is shown in Figure 5.9. It is clear that an unstable system can be predicted to be stable if the tolerance is too large. It is concluded that a pressure boundary tolerance equal to or less than 10^{-6} MPa yields a converged solution, and should be used in the numerical simulations.

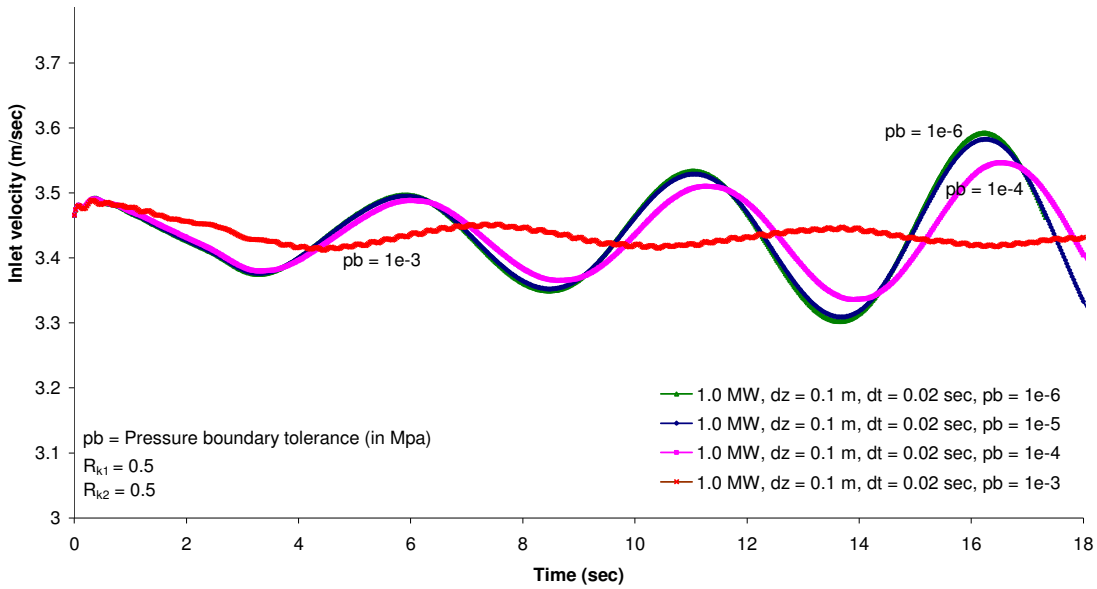

Figure 5.9: Effect of pressure boundary tolerance at 1.0 MW

5.4 Stability boundary

To locate the stability threshold (boundary) on the steady state flow-power curve, applied power is incrementally varied, and the time-dependent set of conservation equations are numerically solved with the temporal and spatial grid size of 0.02 sec and 0.1 m respectively, until the power level where sustained or growing oscillations are obtained. Spatial grid size was retained as 0.1 m to predict the stability limit as reducing it further did not show any effect on stability, although a shift in oscillations is observed. The tolerance for the exit pressure boundary condition is set at 10^{-6} MPa. Transient solutions for 0.70 MW and 0.80 MW lead to stable and unstable flow oscillations, respectively. Results are shown in Figure 5.10. The stability threshold is hence found to be near 0.75 MW.

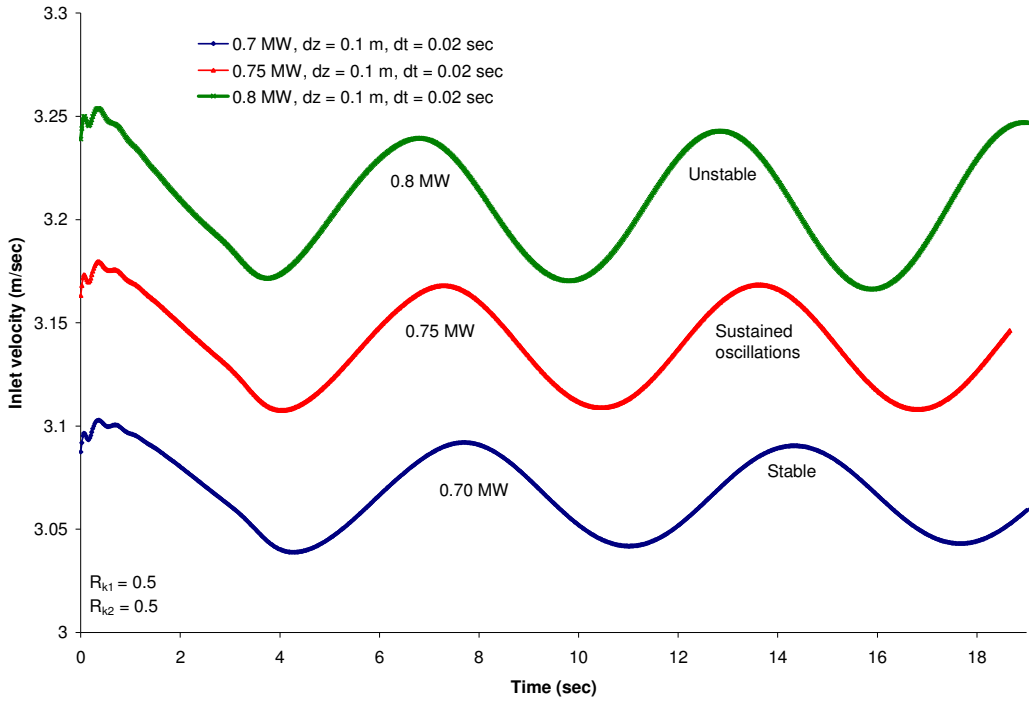

Figure 5.10: Transient solution for three power levels

It must be noted that the results obtained for the stability boundary using the FIASCO code deviate substantially from the results reported in Chatoorgoon et al. (2005c) (see Figure 5.11). The disagreement in results is most likely due to the undesirable dissipative and dispersive effects induced by the large time steps used in reported studies, thereby leading to a larger stable region than those found using smaller time steps. This analysis further shows disagreement with the *near-peak* stability margin region as reported in Chatoorgoon et al. (2005c), and shown in Figure 5.2 (b). Results reported here are also supported by the linear stability analysis of the natural circulation loop, reported in Jain (2005), where it was also concluded that the beginning of instability is not strictly restricted to the peak region of the steady state flow-power curve. Moreover, very recently, Chatoorgoon and Upadhaye (2005a) reported linear stability analysis results for supercritical flow in a natural-convection loop. Though, predicted stability boundaries from this approach were in close agreement to the SPORTS predictions, a significant difference in oscillation periods were reported. Linear solutions always predicted smaller oscillation periods than the SPORTS predictions. Therefore, it is realized that additional

numerical studies for various loop configurations must be performed in order to resolve the inconsistency in different predictions and to accurately identify the stable regime.

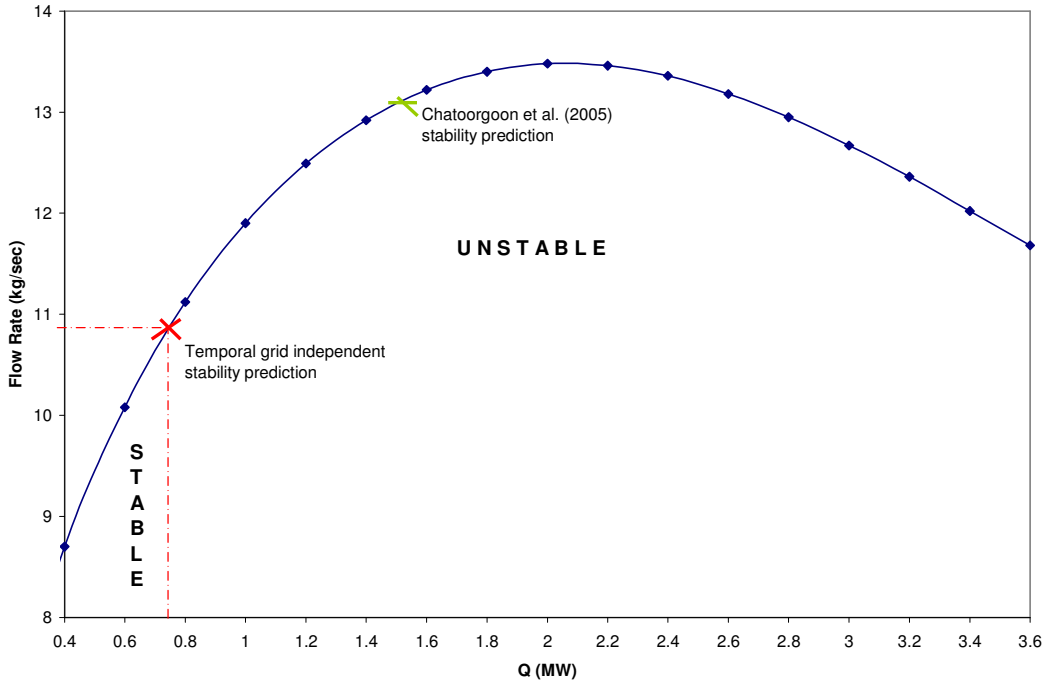

Figure 5.11: Comparison of stability prediction with previous investigations

Chapter 6

Parametric Effects on Stability

The stability characteristics of the CO_2 natural circulation loop are predicted using the FIASCO code for different operating conditions and geometric parameters in order to understand their influence on stability.

6.1 Effect of pressure

For the CO_2 natural circulation loop under supercritical conditions, an increase in system pressure (while keeping other system parameters constant) is found to have a stabilizing effect. Figure 6.1 shows the stability threshold on the flow-power curve for two pressure levels. Changing system pressure from 8 MPa to 10 MPa, increased the threshold power by 0.20 MW to about 0.95 MW.

6.2 Effect of inlet subcooling

Similar to increasing system pressure, an increase in inlet degree of subcooling from 6 C to 16 C leads towards 0.05 MW increase in threshold power and thus stabilizes the flow system, as shown in Figure 6.2. Here, degree of subcooling is defined with reference to the critical temperature of CO_2 (31 C). Unlike the case with pressure increase which leads to a higher flow rate at the new threshold power, an increase in degree of subcooling leads to a lower flow rate at the new stability threshold.

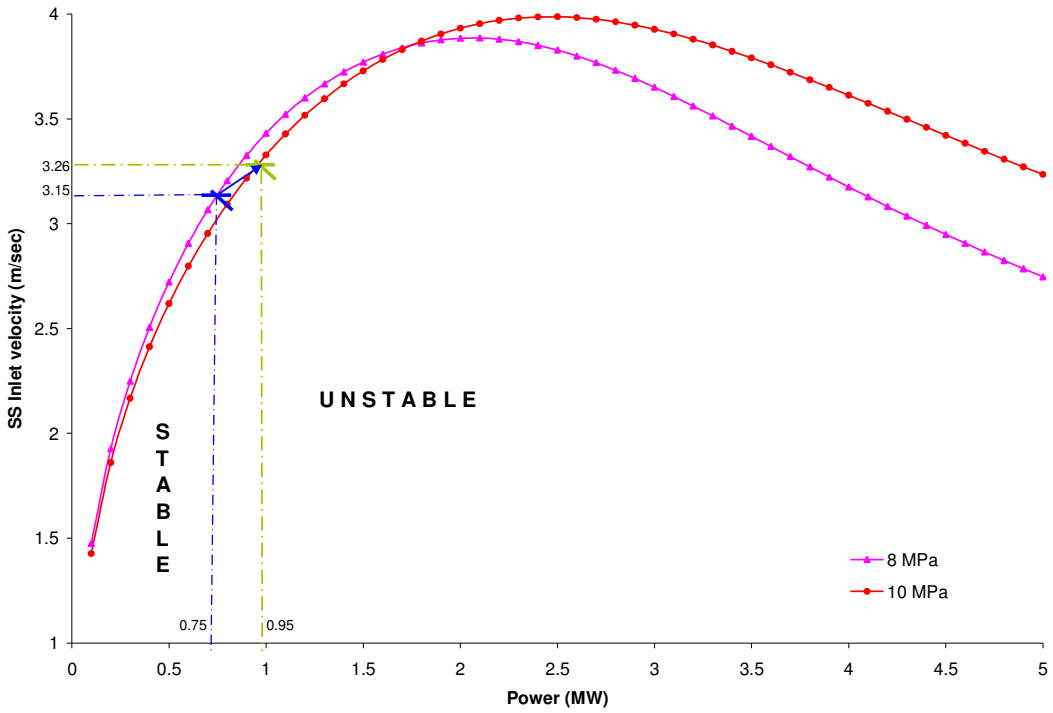

Figure 6.1: Effect of pressure on the stability boundary

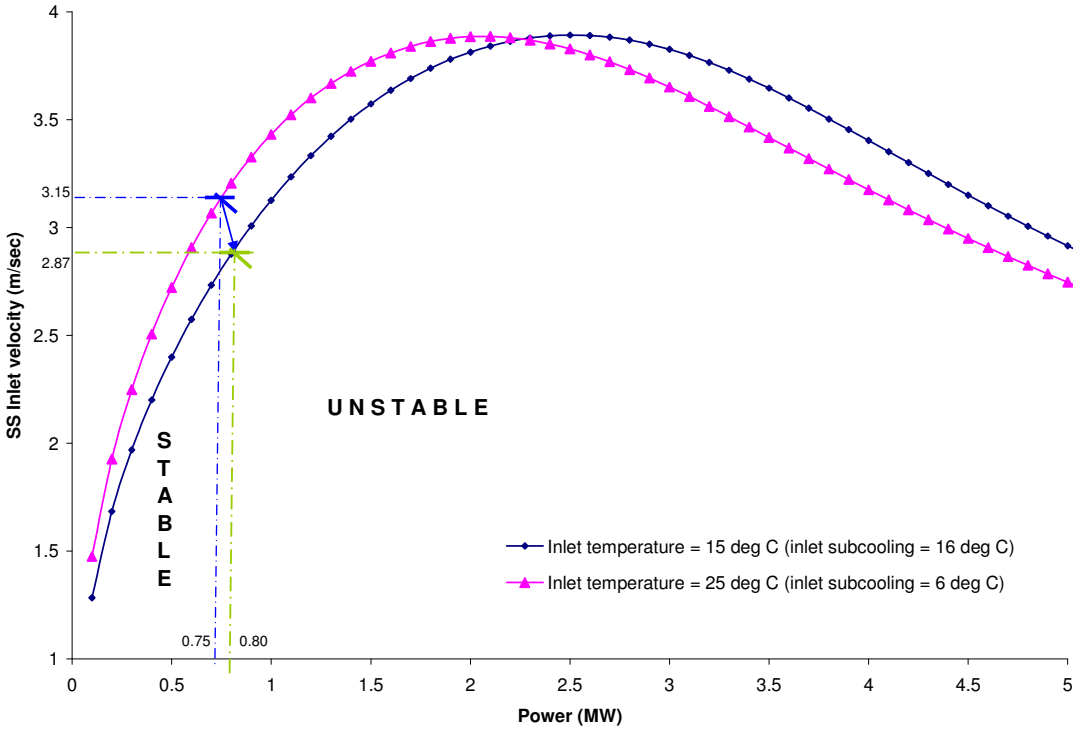

Figure 6.2: Effect of inlet subcooling on the stability boundary

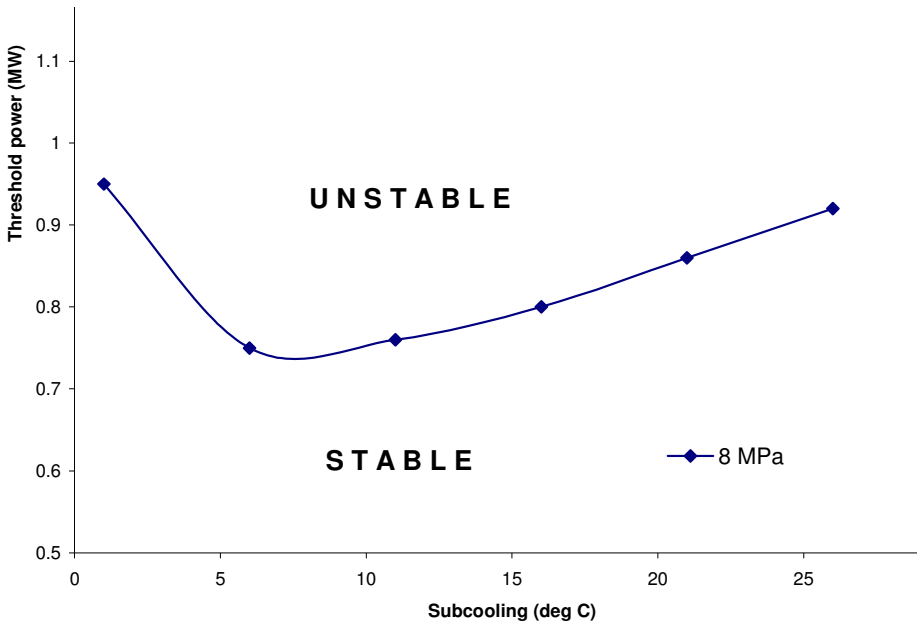

Figure 6.3: Effect of inlet subcooling on threshold power

Figure 6.3 shows the stability boundary plotted in the power-subcooling plane. It is observed that the effect of inlet subcooling on flow stability exhibits a minimum. For small subcoolings, increasing inlet subcooing destabilizes the flow, whereas for high subcooling the effect is stabilizing. Similar behavior is observed in various two-phase heated channel systems (Boure et al., 1973).

6.3 Comparison with boiling two-phase flow systems

Results presented above for the natural circulation loops under supercritical conditions are similar to those reported in the literature for two-phase heated channels and natural circulation systems.

Figure 6.4 shows the steady-state behavior of a two-phase reactor thermosyphon system simulated using different models for two-phase flows. All the models predict a similar trend for the variation of the natural circulation flow rate with power, i.e. flow rate initially rises due to an increase in buoyancy force and then reduces due to an increase in two-phase resistance at higher void fraction (Nayak et al., 2006).

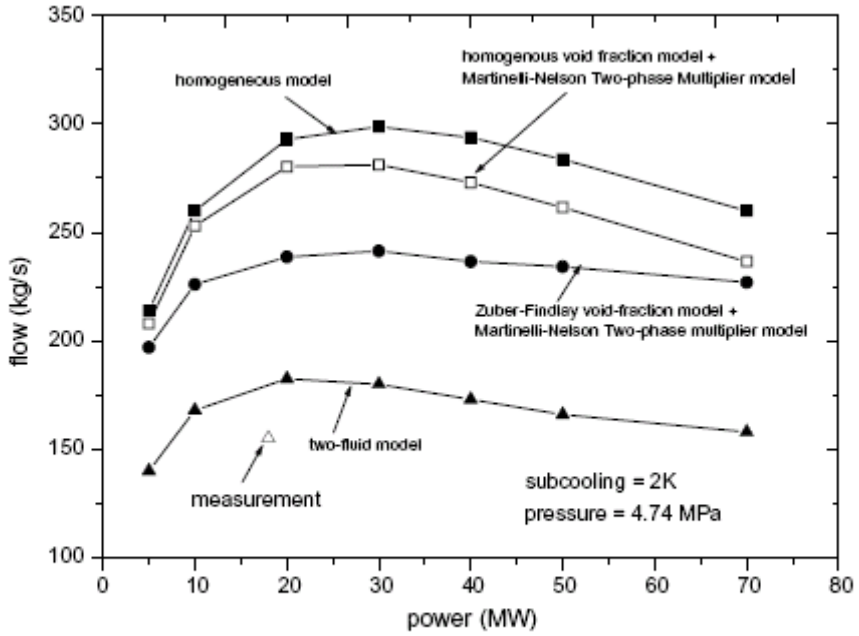

Figure 6.4: Steady state characteristics of a two-phase natural circulation system inside a reactor (Nayak et al., 2006)

The effect of pressure on flow stability during natural circulation with two-phase flow is shown in Figure 6.5. It may be observed that onset of instability occurs on the negative slope region of the steady state flow–power curve. This is different from the supercritical fluid case, where it generally occurred on the positive slope region for the range of parameters studied. Moreover, increase of power input reduces the flow stability; and stability can be induced into the system by increasing the system pressure (Boure et al., 1973).

Similar to the supercritical fluid loop, the increase of inlet subcooling stabilizes the two-phase boiling flow at medium or high subcoolings; while it destabilizes the flow at small inlet subcoolings. Thus, the effect of inlet subcooling on threshold power exhibits a minimum as shown in Figure 6.6 for different system pressures (Boure et al., 1973).

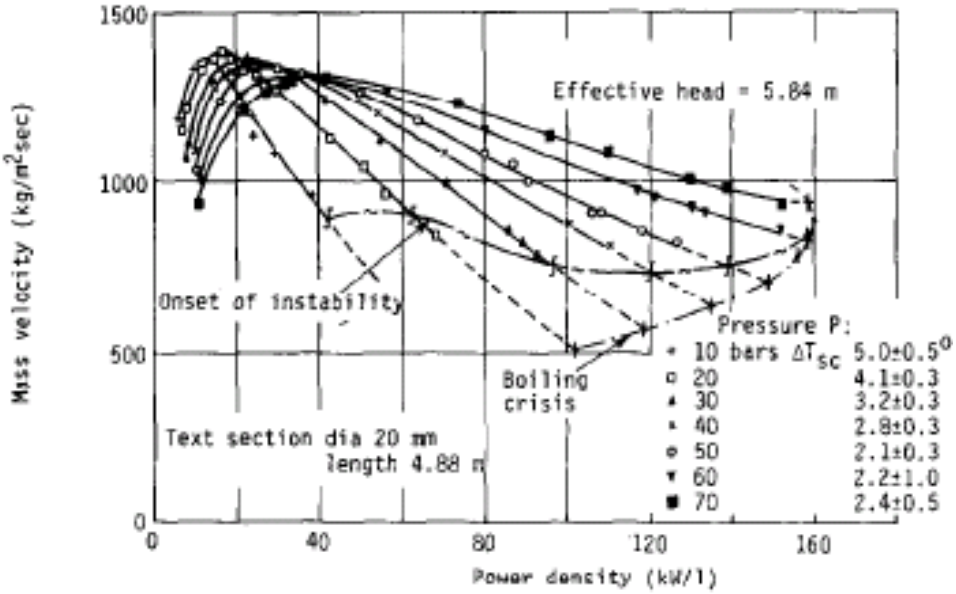

Figure 6.5: Effect of pressure on flow rate under natural circulation of two-phase flow (Boure et al., 1973)

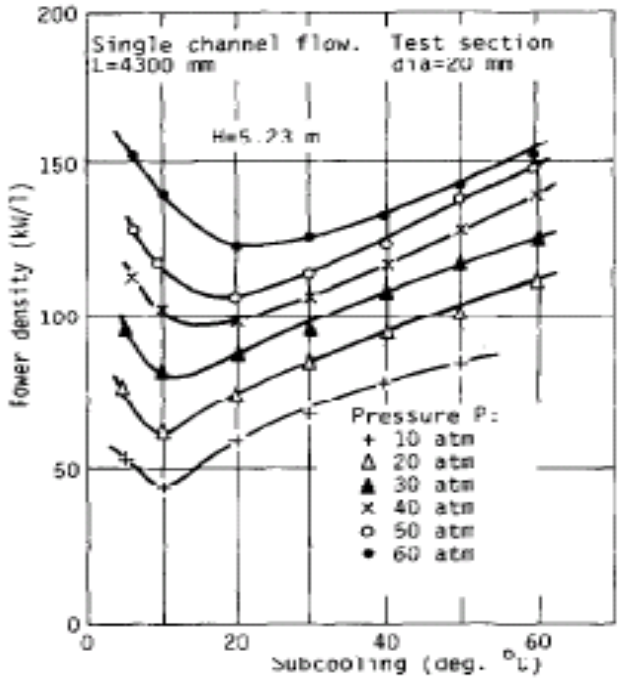

Figure 6.6: Effect of inlet subcooling and pressure on flow instability in a single boiling channel (Boure et al., 1973)

Chapter 7

Summary, Conclusions and Future Work

7.1 Summary and conclusions

Thermal hydraulic instabilities resulting in flow oscillations are highly undesirable in SCWR systems, as they may give rise to nuclear instabilities (due to density-reactivity feedback) and result in failure of control mechanism or fatigue damage of reactor components. That, in turn, will affect the heat removal system efficiency and may put the safety of reactor system in jeopardy. Moreover, employment of passive safety mechanisms, for example, natural circulation cooling systems, requires study of SCWR stability under natural circulation conditions. The natural circulation loop with supercritical flow conditions ─ that always remains in single phase ─ experiences a rather large density change across a very small temperature range near the pseudo-critical point. This may lead the system towards instabilities similar to those observed in heated channels with two-phase flows. A study of flow stability phenomena in a natural circulation loop with supercritical fluid has been carried out in this thesis, which may later be modified to analyze SCWR instabilities as well.

Steady state and dynamic analyses of SCWR require appropriate modeling of the thermodynamic and transport properties of water near its critical point. For this preliminary investigation, a single-channel, one-dimensional model has been developed. In this model, equations for the conservation of mass, momentum and energy have been discretized using an implicit control volume scheme. Thermophysical properties of the supercritical fluid have been determined using the NIST property packages.

A computer code called FIASCO (Flow Instability Analysis under SuperCritical Operating conditions) has been developed in FORTRAN90 to simulate the dynamics of a natural circulation loop with supercritical fluid. Furthermore, this code has been validated by successful reproduction of some of the results available in the literature.

Stability boundary results for the CO_2 natural circulation loop substantially deviate from the results reported by previous investigators, and thus contradict some of the reported findings. The disagreement in results is most likely due to the undesirable dissipative and dispersive effects produced from the large time steps used in previous studies, which led to a larger stable region than those found using smaller time steps. Results presented in this thesis suggest that the stability boundary of a natural circulation loop with supercritical fluid is not confined to the *near-peak region* of the (steady state) flow-power curve.

Additional and more extensive experimental data are needed to resolve the differences between results obtained here and those reported earlier. However, results obtained for the range of parameter values used in this investigation always predict the stability threshold to be on the positive slope region of the (steady state) flow-power curve. Parametric studies for different operating conditions reveal the similarity of stability characteristics under supercritical conditions with those in two-phase flows.

7.2 Future work and recommendations

- Due to lack of experimental studies performed with supercritical fluids in a natural circulation loop, presently there are not enough experimental data available to benchmark numerical findings. Therefore, more experimental studies should be carried out in order to support the numerical work.
- To avoid the numerical inconsistencies and uncertainties associated with time domain stability analysis, a generalized linear stability model should be developed to predict natural circulation loop behavior under supercritical operating

conditions. Although similar models have been developed and reported in Jain (2005) and Chatoorgoon and Upadhye (2005a), inconsistencies still remain in predicting stability behavior as reported results consistently deviate from the experimental findings.

- Developed model is easily extendable in time-domain to predict the onset of density-wave instability in reference design of SCWR by considering equivalent fuel channel with or without water rods.
- In order to accurately simulate the experimental stability predictions of the ANL CO2 loop (Lomperski et al., 2004) as well as the University of Wisconsin-Madison SCW loop (Jain, 2005), the assumption of fluid reservoir at the inlet and exit of flow channel should be relaxed by the application of periodic boundary conditions. It may be done by guessing all the property variables at the inlet of the flow channel, marching towards the end of the channel and match all the variables at the exit with the inlet ones for each time step. However, this approach will be computationally inefficient and highly time consuming.

References

Boure, J. A., Bergles, A. E., Tong, L. S., 1973. Review of two-phase instability. Nucl. Eng. Des. 25, 165-192.

Buongiorno, J. 2004. The supercritical water cooled reactor: ongoing research and development in the U.S. Proceedings of ICAPP'04, Pittsburgh, PA USA, June 13-17, 2004. Paper 4229.

Chatoorgoon, V., 1986. A simple thermalhydraulic stability code. Nucl. Eng. Des. 93, 51-67.

Chatoorgoon, V., 2001. Stability of supercritical fluid flow in a single-channel natural-convection loop. Int. J. Heat Mass Transfer 44, 1963-1972.

Chatoorgoon, V., Upadhye P., 2005a. Analytical studies of supercritical flow instability in natural convection loops. Proceedings of the 11th International Topical Meeting on Nuclear Reactor Thermal-Hydraulics (NURETH-11), Avignon, France, October 2-6, Paper 165.

Chatoorgoon, V., Voodi, A., Fraser, D., 2005b. The stability boundary for supercritical flow in natural convection loops, part I: H_2O studies. Nucl. Eng. Des. 235 (24), 2570-2580.

Chatoorgoon, V., Voodi, A., Upadhye, P., 2005c. The stability boundary for supercritical flow in natural convection loops, part II: CO_2 and H_2. Nucl. Eng. Des. 235 (24), 2581-2593.

Generation IV International Forum (GIF), 2002. A technology roadmap for the Generation IV nuclear energy systems. GIF-002-00.

Harvey, A.H., Peskin, A.P., Klien, S.A., 2004. NIST/ASME Steam Properties, version 2.21. US Department of Commerce, Technology Administration, National Institute of Standards and Technology.

Jain, R., 2005. Thermal-hydraulic instabilities in natural circulation flow loops under supercritical conditions. PhD Thesis, University of Wisconsin Madison, USA.

Lemmon, E.W., McLinden, M.O., Huber, M.L., 2002. NIST Reference Fluid Thermodynamic and Transport Properties – REFPROP, version 7.0. US Department of Commerce, Technology Administration, National Institute of Standards and Technology.

Leuba, J., Rey, J. M., 1993. Coupled thermohydraulic-neutronic instabilities in boiling water nuclear reactors: a review of the state of the art. Nucl. Eng. Des. 145, 97-111.

Lomperski, S., Cho, D., Jain, R., Corradini, M. L., 2004. Stability of a natural circulation loop with a fluid heated through the thermodynamic pseudocritical point. Proceedings of ICAPP'04, Pittsburgh, PA, USA, June 13-17, Paper 4268.

Nayak, A. K., Lathouwers, D., van der Hagen, T. H. J. J., Schrauwen, F., Molenaar, P., Rogers, A., 2006. Applied thermal engineering 26, 644-653.

Pioro, I.L., Khartabil, H.F., Duffey, R.B., 2004. Heat transfer to supercritical fluids flowing in channels ─ empirical correlations (survey). Nucl. Eng. Des. 230, 69-91.

Rizwan-uddin, 1994. Effects of double-humped axial heat flux variation on the stability of two-phase flow in heated channels. Int. J. Multiphase Flow 20 (6), 1129-1142.

Tong, L.S., Tang, Y.S., 1997. Boiling heat transfer and two-phase flow. Second edition, Taylor and Francis.

Voodi, V. A., 2004. Analytical study of non-dimensional parameters governing supercritical flow instabilities. MSc Thesis, University of Manitoba, Canada.

Wang, F. S., Hu, L. W., Pan C., 1994. Thermal and stability analysis of a two-phase natural circulation loop. Nucl. Sci. Eng. 117, 33-46.

Yamagata, K., Nishikawa, K., Hasegawa, S., Fujii, T.,Yoshida, S., 1972. Forced convective heat transfer to supercritical water flowing in tubes. Int. J. Heat Mass Transfer 15, 2575-2593.

Yamaji, A., Oka, Y., Koshizuka, S., 2005. Three-dimensional core design of high temperature supercritical-pressure light water reactor with neutronic and thermal-hydraulic coupling, Journal of nuclear science and technology 42 (1), 8-19.

Yang, W. S., Zavaljevski, N., 2003. Preliminary investigation of power-flow instabilities of supercritical water reactor, ANL, Technical Report.

Yang, W. S., Zavaljevski, N., 2004. Effect of water rods and heat transfer correlations on SCWR stability, ANL, Technical Report.

Zappoli, B., 2003. Near-critical fluid hydrodynamics. C. R. Mecanique 331, 713-726.

Appendix A

Classification of Flow Instabilities

Flow System Instabilities

Static

Simple

- Ledinegg (flow excursion) instability: occurs when the slope of a channel's inherent pressure-drop versus flow curve is more than the slope of the similar external characteristic curve. It could be a pump flow characteristic, or a constant pressure drop system and constant flow delivery system [Equation 1.1]. It is characterized, by an abrupt large amplitude excursion to a new stable operating condition)
- Thermal (boiling crisis): Caused by significant decrease in heat transfer coefficient. It leads to wall excursion with possible flow oscillations.
- Flow regime transition instability: cyclic transitions between bubbly to annular flow could cause flow rate variations
- Interfacial instabilities: Kelvin-Helmholtz instability arise at the interface of two fluids of different densities flowing horizontally with different velocities.
- Burnout and Quenching

Compound

- Unstable vapor formation (bumping, geysering, vapor burst): It is caused by periodic regulation of "metastable" condition, usually due to lack of nucleation sites. It results in sporadic or periodic liquid superheat and violent vaporization with possible expulsion and refilling
- Condensation chugging: caused by bubble growth and condensation followed by surge of liquid. It can lead to periodic interruption of vent steam flow due to condensation and surge of water up to a downcomer.

Dynamic

Simple

- Acoustic Oscillations: caused by resonance of pressure waves. They are characterized by high-frequency pressure oscillations (10-100 Hz) related to the time required for pressure waves to propagate in the system
- Density wave oscillations: These are due to the delay and feedback effects in relationship among flow rate, density and pressure drops. They are marked by low frequencies (~1 Hz) related to the time required for transport of fluid in the systems.

Compound

- Thermal oscillations: The underlying mechanism is the interaction of variable heat transfer coefficient with the flow dynamics. It occurs close to the flilm boiling point.
- Boiling water reactor (BWR) instability: Due to the void-reactivity coupling. It is relevant only for small fuel time constant and low pressure.
- Parallel channel instability: caused by interaction among a small number of parallel flow channels and results in dynamic flow redistribution.
- Condensation oscillation: This is caused by the interaction of direct contact condensation interface with pool convection. It occurs with steam injection into vapor suppression pool.
- Pressure drop oscillation: A flow excursion instability can induce dynamic interaction between a channel and a compression volume leading to a pressure drop oscillation. It is characterized by very low frequencies (~0.1 Hz).

Figure A.1: Classification of flow instabilities in thermal-hydraulic systems (Jain, 2005)

Appendix B

NIST Property Database

In this report, NIST/ASME Steam Properties v. 2.21 (Harvey et al., 2004) and NIST REFPROP v. 7 (Lemmon et. al., 2002) FORTRAN codes have been used to compute thermophysical properties of water and CO_2 respectively, at supercritical conditions. The National Institute of Standards and Technology (NIST) developed the above mentioned code packages to make available different fluids properties in a user-friendly form over a wide range of conditions including supercritical properties. Below is a brief description of both the software packages and directions to execute (or call) different thermophysical properties in a computer code.

B.1 NIST Database 10: NIST/ASME Steam Properties 2.21

This package uses the 1995 version of "Formulation for the Thermodynamic Properties of Ordinary Water Substance for General and Scientific Use", issued by the International Association for the Properties of Water and Steam (IAPWS), to calculate thermodynamic properties of water. All thermodynamic properties of interest in the supercritical region can be computed by this database including temperature, pressure, density, enthalpy and dynamic viscosity. However, due to unphysical behavior of some of the "derivative" properties (for example, the isothermal compressibility, the isochoric and isobaric heat capacities, and the speed of sound) at the pseudo-critical point, computed properties in a region close to the critical point may not be as accurate as in the rest of the region (Harvey et al., 2004). Having access to the source codes for this property database enables property computations by calling the appropriate subroutines directly into any external computer program. All the source codes for the property computations are written in the FORTRAN 77 language, but are compatible with FORTRAN 90/95 (Harvey et al., 2004).

B.2 NIST Database 23: NIST REFPROP 7.0

NIST Reference Fluid Thermodynamic and Transport Properties – REFPROP is a software package developed and supported by the "NIST Physical and Chemical Properties Division and the NIST Standard Reference Data Program". Comparing with the STEAM version, this database provides tables, plots as well as calling subroutines for the thermophysical properties of most of the industrially important fluids and their mixtures (for example, ammonia, CO_2, methane, nitrogen and many more). It is based on the most accurate pure fluid and mixture models available. These models are implemented in specifically developed FORTRAN subroutines to calculate the thermodynamic and transport properties at a given state (Lemmon et. al., 2002). While implementing this database to predict properties, the user must be aware of the uncertainties in the calculated properties that considerably depend on the fluid, property and the thermodynamic state (Lemmon et. al., 2002).

Curriculum Vitae

Prashant Jain received his B.Tech. in Mechanical Engineering from Indian Institute of Technology (IIT) Bombay, India in August 2004. Upon completion of his M.S. in Nuclear Engineering from University of Illinois at Urbana - Champaign, he is looking forward to pursuing his Ph.D. in nuclear engineering.

Right from his childhood, Prashant developed keen interest in sciences and excelled in every step of his education. Throughout his schooling, he consistently ranked among the top few of his class. He was awarded certificate of merit by the Ministry of Human Resources & Development (Department of Education), Government of India in recognition of his outstanding performance in the Secondary and Higher Secondary School Examinations. He was among the top 0.4 % of 150,000 students who took the Joint Entrance Examination (JEE) conducted for admission to the IITs (Indian Institute of Technology), the premier institutes of Engineering and Technology in India.

He was attracted towards Mechanical Engineering because of its fundamental nature and practical applicability in all spheres of life. His four years of undergraduate study at IIT has exposed him to a wide gamut of subjects, including Solid Mechanics, Design, Controls, Dynamics, Thermal and Fluid Sciences, and other interdisciplinary programs, and this has created in him a fine overall blend of Engineering.

At the University of Illinois, Prashant was recognized as a Sargent and Lundy Fellow for the term 2005-06. He was also awarded the membership for the Alpha Nu Sigma nuclear engineering honor society. Along with excelling in the coursework as a graduate student, he also indulged himself in various projects related to innovation in distance education and was exposed to the state-of-the-art technology of Virtual Reality.

Publications and presentations Prashant has authored, co-authored, or presented follow.

- Suneet Singh, **Prashant Jain**, Rizwan-uddin, "Analytical solution to transient heat conduction in polar coordinates with multiple layers in radial direction", Under Review in International Journal of Thermal Sciences (2006)
- E. Edwards, A. Sweet, M. Blanford, R. Agasie, **Prashant Jain**, Rizwan-uddin, "Distance reactor laboratory and virtual tours", Trans. ANS Annual Meeting, Reno, USA, June 4-8 (2006)
- **Prashant Jain**, J. Stubbins, Rizwan-uddin, "Broadcasting nuclear engineering laboratories – video and data – in real-time over the internet", Proc. ASEE Annual Conf., Chicago, USA, June 18-21 (2006)
- **Prashant Jain**, Rizwan-uddin, "Steady-state and dynamic analyses of supercritical CO2 natural circulation loop", Proc. ICONE-14, Miami, Florida, USA , July 17-20 (2006)
- **Prashant Jain**, J. Stubbins, Rizwan-uddin, "Interactive virtual laboratory for distance education in nuclear engineering", Proc. PHYSOR topical meeting, Vancouver, Canada, Sept 10-14 (2006)
- Kyung-doo kim, **Prashant Jain**, J. Stubbins, Rizwan-uddin, "On-line web simulation of system codes", Proc. International Topical Meeting on Nuclear Plant Instrumentation, Control and Human-Machine Interface Technologies, Albuquerque, USA, Nov 12-16 (2006)
- **Prashant Jain**, S. Markidis, B. G. Jones, Rizwan-uddin, J. R. White, L. Bobek, "Web-casting of Nuclear Reactor Experiments", To be presented in ANS Winter Meeting and Technology Expo, Albuquerque, USA, Nov 12-16 (2006)
- **Prashant Jain**, "LabVIEW-Based, Interactive Virtual Laboratory for Nuclear Engineering Education", Proc. ANS Student Conf., Troy, USA, March 30 – April 1 (2006)
- **Prashant Jain**, "Development of a real-time web-casting interface for system codes", Proc. ANS Student Conf, Troy, USA, March 30 – April 1(2006)